

UNIVERSITY OF THE WITWATERSRAND

MASTERS THESIS

**H.E.S.S Data Analysis of Gamma-Ray
Binaries: HESS J0632+057 and LMC P3**

Author:
Johannah MOEPI

Supervisor:
Prof. Nukri KOMIN

*A thesis submitted in fulfillment of the requirements
for the degree of Master of Science*

in the

School of Physics

May 8, 2020

Declaration of Authorship

I, Johannah MOEPI, declare that this thesis titled, "H.E.S.S Data Analysis of Gamma-Ray Binaries: HESS J0632+057 and LMC P3" and the work given in it has been solely tackled by myself. I confirm that:

- This work was done mainly while in candidature for a research degree at the University of the Witwatersrand.
- It has been stated clearly where any part of this thesis was done previously and submitted at University of the Witwatersrand or any other Institution for any qualification.
- Regarding any work that has been published by other people, I clearly stated that as well.
- Quotations from other peoples work have been stated with clearly placed quotation marks, making the thesis entirely my own.
- All the main sources that were of assistance to completing my thesis, have been acknowledged.
- For any joint work in this thesis, I stated clearly what they had done and what were my contributions.

Signed:



Date:



“Wonder and passion are a binary star, intimately orbiting each other, and together exerting a unique gravitational force. Sometimes we seize the moment, and sometimes it seizes us ”

Gregg Levoy

Abstract

Johannah MOEPI

H.E.S.S. Data Analysis of Gamma-Ray Binaries: HESS

J0632+057 and LMC P3

Context: Gamma-ray binaries consist of a normal star and a neutron star or a black hole orbiting around the same centre of mass. This interaction produces emission of gamma rays which dominates the electromagnetic spectrum. In this research we take a close look at two gamma-ray binaries HESS J0632+057, located near Rosette Nebula and the Monoceros Loop, and LMC P3, which is the first Extra-Galactic gamma-ray binary located in the satellite galaxy of Milky Way, the Large Magellanic Cloud. Cross-check analysis for H.E.S.S. observations for HESS J0632+057 is required and analysis of newly taken data for LMC P3 requires preparation, hence the study of the two gamma-ray binaries.

Aim: In order to test that these two binary stars are gamma-ray emitters, periodic emission signatures must be searched for and measured. Therefore the aim of this research is to do a cross-check analysis of HESS J0632+057 using only new and unpublished observations to obtain the average spectrum and do an analysis of phase-folded light-curves to see if there is a periodic modulation. The second aim is to prepare analysis of newly taken data of LMC P3.

Method: There have been observations of the sources in 2004-2012 and the data have been taken by the H.E.S.S. telescopes. Analysis has been done using the standard HESS Model++ software.

Results: There is a detection of the HESS J0632+057 with a statistical significance of 8.6σ . The light-curves were folded on the known period $T_0 = 54857.0$ MJD and $P_0 = 316.2$ days. The folded lightcurve shows a peak of emission in the orbital phase range 0.6 to 0.9. Regarding LMC P3, analysis was not possible because there were issues with instrument response functions. However, the noted errors can be a guide for better analysis techniques.

Conclusion: More data must be taken in order to have enough data points during the periastron passage of HESS J0632+057. Analysis of LMC P3 has been prepared. The analysis shows errors and the calibration of the data set needs to be revisited. New instrument response functions must also be created to fix the error in reading data of the CT5 telescope.

Acknowledgements

I would like to acknowledge my Supervisor Prof Nukri Komin for assisting me throughout my studies, giving me guidance in all the possible ways that I can take in tackling my studies, providing me with invaluable advices that kept me going, promptly answering all the questions and queries that I had every step of the way, and mostly having patience.

To my parents, Moepi Johannes Morake and Moepi Gaamele Francinah, without you I would not be where I am today. You held my hand every step of the way, made me laugh when I felt down, saying 'Thank you for Everything' feels like an understatement but know that I am grateful for all that you have done for me. May the Good Lord of Mount Zion bless you abundantly, May you live long.

To my family, my dear sisters and dear brothers, my uncle, my niece and nephews, thank you for being there for me. Thank you for supporting me and making me believe in myself. May God Bless all of you.

I would also like to thank all the people that motivated me and gave me support in the School of Physics.

Contents

Declaration of Authorship	iii
Abstract	vii
Acknowledgements	ix
1 Introduction	1
1.1 Supernova Explosions of stars	1
1.2 X-ray and Gamma-ray binaries	2
1.2.1 High Mass X-Ray Binaries	2
1.2.2 Low Mass X-ray Binaries	3
1.2.3 Telescopes detecting X-ray binaries	3
1.2.4 Gamma-ray Binaries	4
1.3 The Discovered Gamma-Ray Binary Systems	5
1.4 The powering mechanisms of gamma-ray binaries	8
1.5 The Importance of Gamma-ray Binaries	9
2 Imaging Atmospheric Cherenkov Telescopes	11
2.1 How IACTs operate	11
2.2 IACTs	13
2.3 Imaging Atmospheric Cherenkov Telescope instruments	14
2.3.1 History	14
2.3.2 H.E.S.S	15
2.3.3 VERITAS	15
2.3.4 MAGIC	16
2.4 Analysis Method	16
2.4.1 Theta squared plot	16
2.4.2 How ON and OFF sources are obtained	16
2.4.3 Sky Map	17

2.4.4	Spectrum	17
2.4.5	Light-curve	18
3	The Gamma-Ray Binaries HESSJ0632+057 and LMC P3	21
3.1	HESS J0632+057	21
3.2	LMC P3	25
4	Analysis and Results	27
4.1	Data Sets	27
4.1.1	HESS J0632+057	27
4.1.2	LMC P3	28
4.2	HESS J0632+057	28
4.2.1	Theta squared plot	28
4.2.2	Sky Map	29
4.2.3	Energy Spectrum	29
4.2.4	Lightcurve	32
4.3	LMC P3	32
4.3.1	Initial Analysis	32
4.3.2	Follow-up analysis	36
5	Discussion	39
5.1	HESS J0632+057	39
5.2	LMC P3	40
6	Conclusion	45
	Bibliography	47

List of Figures

1.1	The companion star accretes material of the massive star after it evolved to a point where the Roche-lobe is filled.	3
1.2	Important terminology in binary systems	5
1.3	Pulsar-wind scenario: A Be star with circumstellar disk is orbited by a fast-rotating neutron star.	8
1.4	Microquasar scenario: Massive star accreting material from a compact object(NS/BH). There is an emission of relativistic jets as well.	10
2.1	Left: Primary gamma ray generating Electromagnetic shower. Right: Hadronic particle generating hadronic cascade. Credit: https://link.springer.com/chapter/10.1007/978-88-470-2688-9_4#citeas	11
2.2	Depiction of the operation of Imaging Atmospheric Cherenkov Telescopes(IACTs).	13
2.3	Camera images of the Extensive Air Shower as viewed on the 5 HESS telescopes. Credit: https://www.mpi-hd.mpg.de/hfm/HESS/pages/home/som/2012/12/	14
2.4	How the theta parameter is calculated. Credit: (https://indico.mpp.mpg.de/event/3707/session/14/contribution/51/material/slides/0.pdf)	17
3.1	HESS J0632+057 coincident with MWC 148 located within the Monoceros Loop on the edge of the Rosette Nebula, (Aharonian, 2007)	23
3.2	HESS J0632+057 orbit with periastron phase at 0.967 and apastron phase at 0.467. The dots show 0.1 interval of orbital phase. Credit: Casares et al. (2012)	24
4.1	Distribution of ON(black crosses) and OFF(green shaded region) events from stereo data set HESS J0632+057 and background control regions respectively.	30

4.2	Distribution of ON and OFF events from Mono data set of HESS J0632+057 and background control regions respectively.	30
4.3	Sky map showing the location of HESS J0632 +057 with the ON region marked by the black circle on the centre.	31
4.4	Observed differential flux of gamma rays in HESS J0632+057. The green line shows the power law fit to the data points used from the stereo data set. A list of the best-fit parameters obtained are listed in Table 4.3	31
4.5	Integrated lightcurve of HESS J0632+057 computed with energy above 0.35TeV.	32
4.6	Phase folded lightcurve of HESS J0632+057 computed with $T_0 = 54857.0$ MJD and $P_0 = 316.2$ days.	33
4.7	Theta squared plot of the LMC P3 old instrument response functions with standard shower goodness cut of 0.9. The ON region(black points) and background region(green shaded region) are both distributed in the plot.	34
4.8	Distribution of shower goodness of Crab Nebula real data. Red line shows the ON source events, Blue line shows the background and the green line shows the excess events where the OFF source events are subtracted from the ON source events. This shower goodness was computed with H.E.S.S.Paris Analysis old instrument response functions.	34
4.9	Distribution of ON(black crosses) and OFF(green shaded region) events from custom analysis of LMC P3 and its background control regions. Reflected background model was used to produce the squared angular distribution.	35
4.10	LMC P3 old instrument response functions sky map showing the location of it with the 'ON' region marked by the black circle on the centre. Left plot is the excess map and the right plot is the significance map	35

4.11	Distribution of ON(black crosses) and OFF(green shaded region) events from the Stereo_HESSI_standard analysis of LMC P3 and its background control regions with new instrument response functions. Reflected background model was used to produce the squared angular distribution. The theta squared plot is for the modified cuts.	37
4.12	LMC P3 sky map produced from 4 telescopes showing the location of the source with no gamma-ray detection	37
5.1	Published lightcurve from Maier et al. (2019)	41

List of Tables

1.1	Different types of compact stars.(Postnov and Yungelson, 2014)	1
1.2	The family of gamma-ray binaries arranged by orbital period. Parameters are from: LS 5039 (Casares et al., 2005a); 1FGL J1018.6-5856 (Corbet et al. (2011), Napoli et al. (2011)); LS I +61 303 (Aragona et al., 2009), (Zamanov et al., 1999), (Casares et al., 2005b), (McSwain et al., 2010); HESS J0632+057 (Aragona, McSwain, and De Becker, 2010); PSR B1259-63 (Negueruela et al., 2011), (Johnston et al., 1994). LMC P3 parameters were obtained from van Soelen et al. (2019). PSR J2032+4127 (Abeysekara et al., 2018). M_{opt} : Mass of the optical star. i : Inclination angle of the plane of the orbit relative to the plane that is perpendicular to the line of sight from the Earth to the body. p_{orb} : Orbital period. e : Orbital eccentricity. $a(1-e)$: Periastron, obtained from semi-major axis(a) and the eccentricity(e). $a(1+e)$: Apastron, obtained from semi-major axis(a) and the eccentricity(e). d : Distance from the gamma-ray binary system to earth.	7
4.1	Detailed description of the configurations used in the study for the two data sets of HESS J0632+057. For mono data set, new runs were used. They are with the new upgraded "HESSIU" cameras. From the stereo data set, old and new runs were used. Old runs corresponds to the original cameras for the HESSI telescopes.	28
4.2	VHE γ -ray Statistics of HESS J0632+057. MA - Model analysis. Non - number of events in on source region, Noff - number of events in off source region, alpha - background normalisation, depends on the number of off-source regions.	29
4.3	Spectral Parameters of HESS J0632+057	29
4.4	VHE γ -ray Statistics of LMC P3 with standard instrument response functions	35

4.5 Fit values of the mean Shower goodness of gamma rays for Crab Neb-
ula computed with old instrument response functions. The constant
corresponds to the amplitude, the mean corresponds to the shift and
the sigma corresponds to the width. 36

List of Abbreviations

HESS	High Energy Stereoscopic System
MAGIC	Major Atmospheric Gamma Imaging Cherenkov telescope
VERITAS	Very Energetic Radiation Imaging Telescope Array System
VHE	Very High Energy
HE	High Energy
MJD	Modified Julian Date
UV	Ultra-Violet
ISM	Interstellar Medium
HMXB	High Mass X-ray Binary
LMXB	Low Mass X-ray Binary
IMXB	Intermediate Mass X-ray Binary
WD	White Dwarf
NS	Neutron Star
BH	Black Hole
FWHM	Full Width (at) Half Maximum
COSB	Cosmic Origins Spectrograph-B
EGRET	Energetic Gamma Ray Experiment Telescope
IACT	Imaging Atmospheric Cherenkov Telescope
EAS	Extensive Air Showers
EM	Electro Magnetic
HEGRA	High Energy Gamma Ray Astronomy
ATCA	Australia Telescope Compact Array
LMC	Large Magellanic Cloud
SG	Shower Goodness

Chapter 1

Introduction

This chapter gives an introduction to gamma-ray and X-ray binaries.

1.1 Supernova Explosions of stars

The universe is occupied by 68% dark energy, 27% dark matter and $6\% \pm 1\%$ baryonic matter¹ which is in stars and stellar remnants (Fukugita and Peebles, 2004). As a star undergoes its stages of life, there comes a time when the star runs out of fuel in the core hence leading to the core of the star to collapse due to loss of the outward pressure.

The collapsing of the core of a massive star leads to the formation of a neutron star. The collapsing of the core of a very massive star leads to a black hole. In Table 1.1 we can see that a massive star is a star of size $> 8 M_{\odot}$ and a very massive star is a star with mass ranging between $30 M_{\odot}$ and $150 M_{\odot}$. Table 1.1 shows the range of masses of the stars that produce either a white dwarf, neutron star or a black hole.

Names	Initial mass[M_{\odot}]	Remnant type	Mean remnant mass[M_{\odot}]
Low mass star	$0.95 < M < 8-12$	WD	0.6
Massive star	$8-11 < M < 25-30$	NS	1.35
Very massive star	$30 < M < 150$	BH	~ 10

TABLE 1.1: Different types of compact stars.(Postnov and Yungelson, 2014)

¹Baryonic matter is a matter that is made up of baryons(protons, neutrons and atomic nuclei since it is made up of these components)

1.2 X-ray and Gamma-ray binaries

A binary system is when a star forms from the collapse of the progenitor gas cloud that are gravitationally bound.

There is a class of binary stars which are luminous in the X-ray band and they are X-ray binaries. These X-ray binary systems are X-ray sources that produce fluxes ranging between 10^{34} and 10^{38} $\text{erg.cm}^{-2}\text{s}^{-1}$ in the energy range 1-10 keV. All High Mass X-ray Binaries (HMXB) are driven by accretion and these systems consists of stars that lose mass into a compact object, either a neutron star or a stellar-mass black hole. With X-ray observations of these systems we can study the compact objects' nature and properties. Charles and Coe (2003) have reviewed previous papers that have shown that in optical wavelengths, the mass-donor star was studied. The X-ray binary class consists of three subclasses: high-mass X-ray binaries (HMXBs), intermediate mass X-ray binaries (IMXBs) and low-mass X-ray binaries (LMXBs). HMXBs consists of companion stars with $M_* \geq 10M_{\odot}$ and the LMXBs consist of companion stars with $M_* < 10M_{\odot}$. The LMXBs originates from the IMXBs. The IMXBs have two components, with one either being a neutron star or a black hole and the other component being an intermediate-mass star. The mechanism driving the accretion for these two subclasses are also not the same. For HMXBs, the process of mass-transfer to compact objects proceed through the capture of stellar wind while for LMXBs accretion is powered by Roche-lobe overflow which occurs when a star fills up its Roche-lobe in a binary system, see Figure 1.1.

1.2.1 High Mass X-Ray Binaries

As a massive star undergoes supernova explosion, an HMXB system is born only if the star was in a Binary System before the explosion.

This subclass of X-ray Binaries can also be divided into another subclass according to the donor's luminosity. There are super-giant X-ray binaries and Be/X-ray binaries. Super-giant binaries contain a young star of O/B type. Be/X-ray binaries have a Oe/Be star as the companion star in the system. The Be star has a circumstellar disk whose optical spectrum typically show a $H\alpha$ emission line. In super-giant

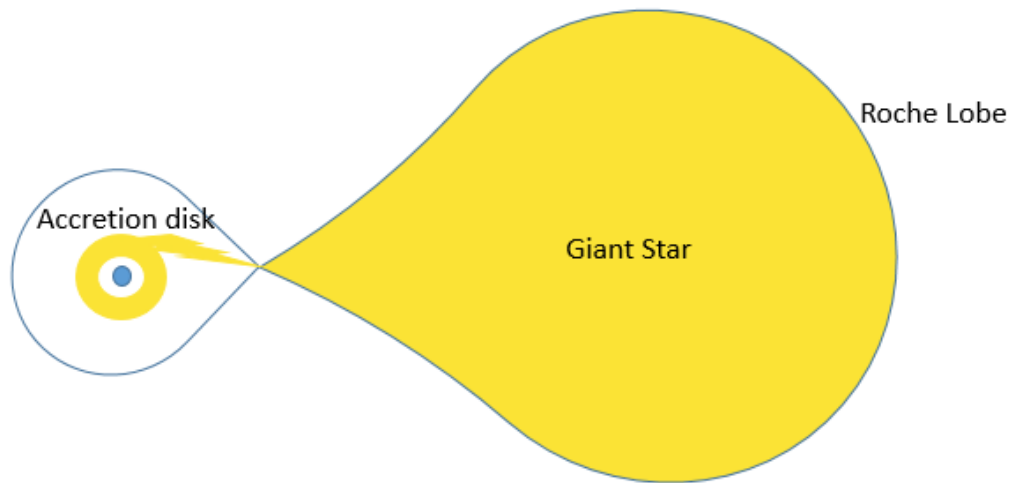


FIGURE 1.1: The companion star accretes material of the massive star after it evolved to a point where the Roche-lobe is filled.

binaries, the accretion happens from the stellar wind, while in Be/X-ray binaries, accretion can also occur from the circumstellar disk.

1.2.2 Low Mass X-ray Binaries

This class of X-ray binaries is characterized by X-rays that reveal short-periods. The orbit of LMXBs is short because the stars in the system are closer together resulting in a short orbital period. They are mostly found in the Galactic Bulge² and Globular clusters³. The LMXBs have a K/M spectral type low-mass donor star and a white dwarf where accretion occurs via Roche-lobe overflow (Figure 1.1). In LMXB, the mass donor is the K/M star which is less massive than the white dwarf compact object. The study behind the birth and formation of LMXB has different theories which can be found in Patterson (1984) and Kalogera and Webbink (1998).

1.2.3 Telescopes detecting X-ray binaries

X-ray binaries are believed to be emitters of gamma rays. Successful X-ray satellites that were built started operating between the 1970s and the 1990s. Gamma-ray emission from X-ray sources was first detected by the COS-B telescope which detected

²The Galactic bulge is a distribution of stars in a spherical shape that is located in the centre of the Milky Way Galaxy and can extend to 3kpc distance from the centre.

³Globular clusters consist of stars that are tightly packed and closer together in space.

strong non-thermal gamma rays and revealed the existence of variable gamma-ray emitters. It could detect gamma rays with energies ranging between 50MeV-5GeV (Hermsen, 1983). As the COS-B telescope detected the strong non-thermal gamma rays, the telescope was observing an unidentified source 2CG 135+01 at energies above 100 MeV (Tavani et al., 1998). This source was consistent with GT 0236+610 which is a radio source, and through the studies found in Gregory et al. (1979), it was revealed that it is LS I 61 303. With limited sensitivity, EGRET could detect it but not detect the variability. EGRET is an instrument on the Compton gamma ray observation which is sensitive in energies ranging between 20 MeV-30 GeV. Its detection mechanism utilizes electron-positron pair production (Hartman et al., 1992).

In 1968, the first Cherenkov telescope, the Whipple telescope, was constructed (Fazio et al., 1968). It detected the Crab Nebula which was the first TeV source ever to be detected (Weekes et al., 1989). After the construction of Whipple, the concept of stereoscopic observations emerged and that led to a new generation of improved Imaging Atmospheric Cherenkov Telescopes (IACTs) in the 2000s. The HEGRA Cherenkov telescopes were located at 28.75°N, 17.89°W on the Canary Island of La Palma (Daum, 1997). The properties of these IACT telescopes (The High Energy Stereoscopic System (H.E.S.S), Major Atmospheric Gamma Imaging Cherenkov telescope (MAGIC) and Very Energetic Radiation Imaging Telescope Array System (VERITAS)) enabled detection of gamma-ray variability.

1.2.4 Gamma-ray Binaries

All gamma ray binaries are high mass binary systems with a compact object that orbits around massive star of type O or Be. They have the peak of emission above 1 MeV (Dubus, 2013). There are 9⁴ gamma-ray binaries detected so far. Gamma-ray emission may be pulsar-wind driven or accretion driven (Mirabel, 2006). A summary of the known systems is given in section 1.3.

The emission of binary systems changes with the orbit of the system. An orbit can be described with the following parameters:

⁴Two of the gamma-ray binaries:4FGL J1405.16119 (Corbet et al., 2019) and HESS J1832-093 (Martí-Devesa and Reimer, 2020) were reported after the submission of the thesis and will not be discussed further.

Periastron: The point of closest separation between the two stars.

Apastron: The point of farthest separation between the two stars.

Inferior Conjunction: Point in the orbit where a compact object is on the side closer to the Earth.

Superior Conjunction: Point in the orbit where a compact object is on the side further from the Earth.

eccentricity: The degree as to how much the orbit deviates from being circular.

See Figure 1.2

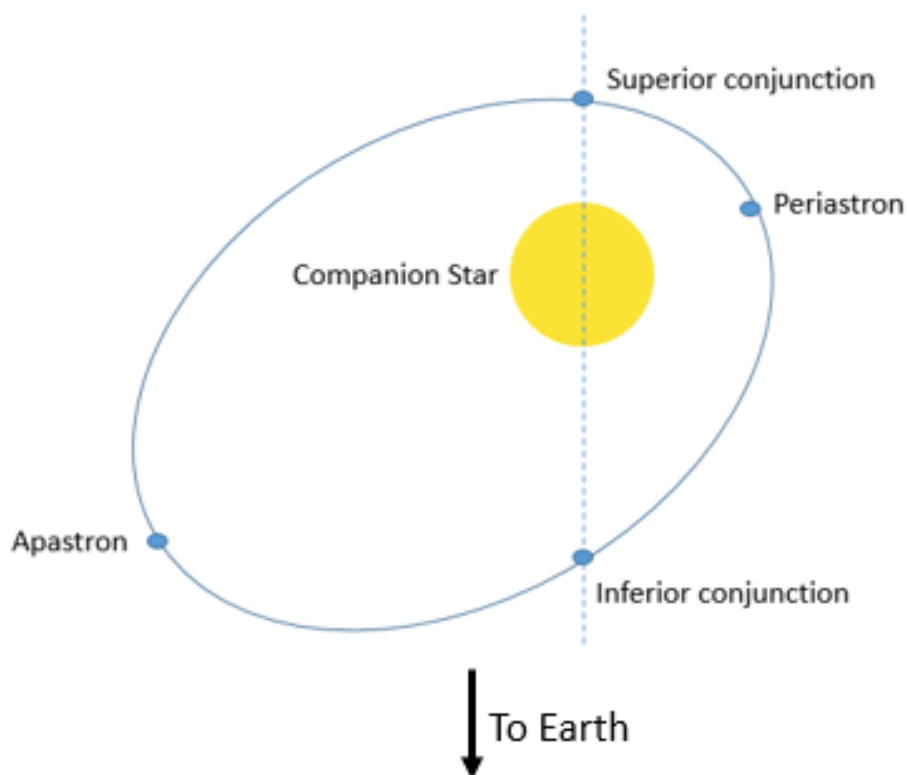


FIGURE 1.2: Important terminology in binary systems

A gamma-ray binary is expected to reveal orbitally varying gamma-ray emission due to the viewing angle and the eccentric orbit changing (C. C. Freire et al., 2012).

1.3 The Discovered Gamma-Ray Binary Systems

After the first discovery of gamma-ray binaries in the mid-2000s by the H.E.S.S., MAGIC and VERITAS collaborations, there are still only 7 gamma-ray binaries known. All of them show variability of gamma rays on the orbital period timescale. They are

point like gamma-ray sources. Some are detected in both Very High Energies ranges from $E > 100$ GeV and High Energies ranges from $100 \text{ MeV} \leq E \leq 100 \text{ GeV}$, see Table 1.2.

1. PSR B1259-63: It is the first observed Galactic source of Very High Energy (VHE) gamma rays which showed variations on a timescale of days (Aharonian, F. et al., 2005; Abdo et al., 2011). It is composed of a massive luminous O9.5Ve star and a neutron star with a spinning period of 47.8 ms in a 3.4 year highly eccentric orbit with an eccentricity of 0.87 (Shannon, Johnston, and Manchester, 2014). H.E.S.S. detected gamma-ray emission during the 2014 periastron passage (Aharonian, F. et al., 2005).

2. LS 5039: This is a both HE (Abdo et al., 2009) and VHE (Aharonian et al., 2005; Aharonian et al., 2006) variable point-like gamma-ray source. The night-by-night light-curve (LC) folded on the 3.9 days orbital period clearly shows its variability. Optical observations have revealed that the source is coincidentally positioned with a massive star of spectral type O6V((f)). Casares et al. (2005a) suggest that it is a microquasar.

3. LS I +61 303: From Swanenburg et al. (1981), LS I +61 303 was identified 35 years ago by COS-B satellite to be a gamma-ray source, but it was first detected by the MAGIC telescope at VHE (Albert et al., 2006b). Massi et al. (2004) thought that it was the first detected microquasar at VHE. Frail and Hjellming (1991) showed that it is a Be star, specifically a B0V main sequence star having a circumstellar disk with a compact object of unknown nature orbiting around it. HE emission are detected across the whole orbit (Hadasch et al., 2012).

4. 1FGL J1018.6-58.56: It is a binary system that was first detected by Fermi LAT in HE (GeV) (Corbet et al., 2012). The system consists of an unknown compact object and an O-type star in a 16.6-day orbit. It was detected at VHE by H.E.S.S (Abramowski, 2015).

5. HESS J0632+057: It is the only gamma-ray binary to be discovered in VHE

(Aleksić et al., 2012; Aharonian, 2007). It is a binary system that has a Be-star companion and unknown compact object with an orbital period of 316.2 days. It has variable very high energy emission. This is the gamma-ray binary that is studied in detail in this thesis. A more detailed discussion is given in, go to Chapter 2 and Chapter 5.

6. LMC P3: This is the first extra-galactic binary system to be discovered. It has an orbital period of 10.3 days (Corbet et al., 2016). VHE gamma ray emission has been detected only between the orbital phases 0.2 and 0.4 (HESS Collaboration et al., 2018). For a more detailed discussion, go to Chapter 2 and Chapter 5.

7. PSR J2032+4127: Abeysekara et al. (2018) recently observed this gamma-ray binary at a recent periastron that occurred on 13 November 2017. It has a period of 50 years.

TABLE 1.2: The family of gamma-ray binaries arranged by orbital period. Parameters are from: LS 5039 (Casares et al., 2005a); 1FGL J1018.6-5856 (Corbet et al. (2011), Napoli et al. (2011)); LS I +61 303 (Aragona et al., 2009), (Zamanov et al., 1999), (Casares et al., 2005b), (McSwain et al., 2010); HESS J0632+057 (Aragona, McSwain, and De Becker, 2010); PSR B1259-63 (Negueruela et al., 2011), (Johnston et al., 1994). LMC P3 parameters were obtained from van Soelen et al. (2019). PSR J2032+4127 (Abeysekara et al., 2018). M_{opt} : Mass of the optical star. i : Inclination angle of the plane of the orbit relative to the plane that is perpendicular to the line of sight from the Earth to the body. p_{orb} : Orbital period. e : Orbital eccentricity. $a(1-e)$: Periastron, obtained from semi-major axis(a) and the eccentricity(e). $a(1+e)$: Apastron, obtained from semi-major axis(a) and the eccentricity(e). d : Distance from the gamma-ray binary system to earth.

Name	gamma-ray Activity	Spectral Type	M_{opt} (M_{\odot})	i (deg)	p_{orb} (days)	e	$a(1-e)$ (AU)	$a(1+e)$ (AU)	d (kpc)
LS 5039	HE,VHE	O6.5V((F))	20-26	13-64	3.91	0.35	0.09	0.19	2.5
1FGL J1018.6-5856	HE	O6V((F))	~37	-	16.58	-	-	-	~5.4
LS I +61303	HE,VHE	B0 Ve	10-15	10-60	26.50	0.54	0.19	0.64	1.9
HESS J0632+057	VHE	B0 Vpe	13-19	47-80	321	0.83	0.40	4.35	~1.4
PSR B1259-63	HE,VHE	O9.5 Ve	31	19-31	1236.79	0.87	0.93	13.44	2.3
LMC P3	HE,VHE	O5III	50	33.5	10.3				
PSR J2032+4127	VHE	B0Ve	15		50	0.94-0.99			1.4-1.7

1.4 The powering mechanisms of gamma-ray binaries

According to Dubus (2015), the mechanisms powering gamma-ray emission in gamma-ray binaries can be divided into two scenarios:

1. Pulsar wind driven: Are being powered by pulsar rotation
2. Accretion driven: Powered by accretion onto a neutron star or a black hole

The unresolved issue in gamma-ray binaries is the unknown compact object. Out of 7 known gamma-ray binaries there are two systems with a known pulsar, PSR J2032+4127 and PSR B1259-63. PSR B1259-63 has an identified compact object which is a 48ms pulsar. The two scenarios invoked to explain the non-thermal aspect of gamma-ray binaries are summarized below.

Pulsar-wind Scenario

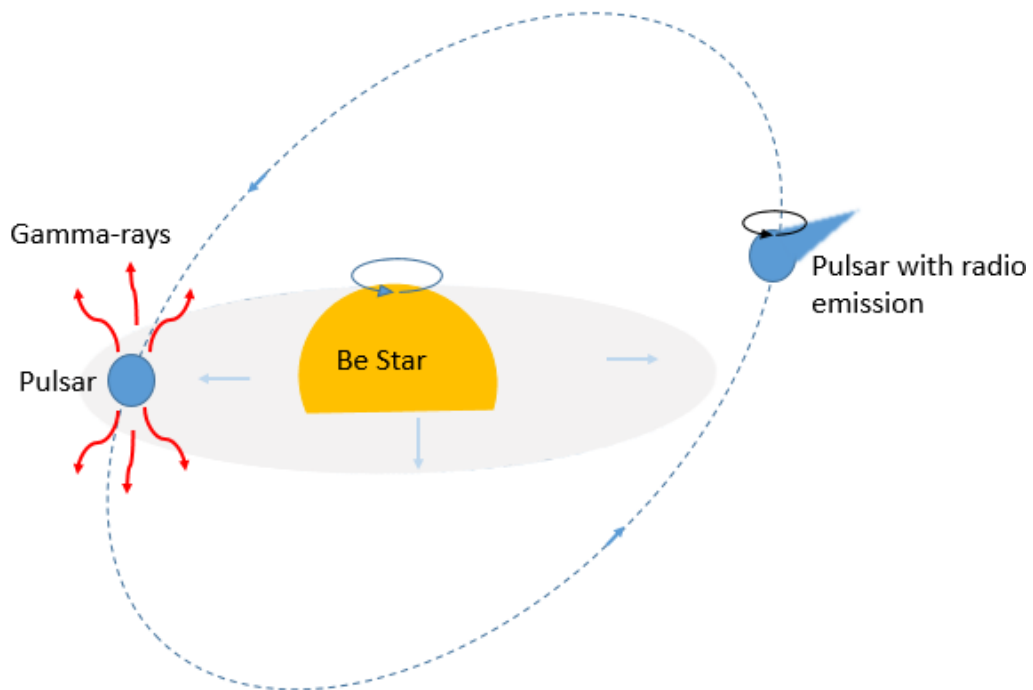


FIGURE 1.3: Pulsar-wind scenario: A Be star with circumstellar disk is orbited by a fast-rotating neutron star.

This scenario, shown in Figure 1.3, involves a rotation-powered pulsar which is highly magnetized and interacting with the stellar wind of a massive star or the circumstellar disk of a Be star. It orbits the massive star in an eccentric orbit. If the pulsar is young, a strong pulsar wind will be created by

its large spin-down luminosity.

A shocked region will be created through the collision of the stellar wind and the pulsar wind. The shocked region will produce gamma ray emission through the Inverse Compton scattering of the stellar photons with relativistic electrons found in the shocked region (e.g. Dubus, Cerutti, and Henri, 2010).

Microquasar Scenario

The microquasar scenario consists of a companion star that loses mass through accretion into the compact object, as shown in Figure 1.4. The accreted material forms an accretion disc and a relativistic jet. From 7 known gamma-ray binaries, LS I +61 303 has the best evidence of being a microquasar however there is no clear consensus (Albert, 2006a). There are different microquasar-based gamma-ray emission models: some regarding hadronic mechanisms and some regarding leptonic mechanisms. For hadronic mechanisms, there is interaction between relativistic protons in the ions with non-relativistic stellar wind ions producing the gamma-rays via neutral pion decay. For leptonic mechanisms, the production of gamma-rays is through inverse compton scattering of relativistic electrons found in the jet on stellar and/or synchrotron photons (Bosch-Ramon et al., 2006).

1.5 The Importance of Gamma-ray Binaries

Gamma-ray binaries offer ways of being able to study how relativistic outflows are formed from highly magnetized, rotating objects (Dubus, 2013). The lightcurves and spectral shapes of these binary stars provide information about where the accelerated particles originate and also give values of the amplitude of the magnetic field.

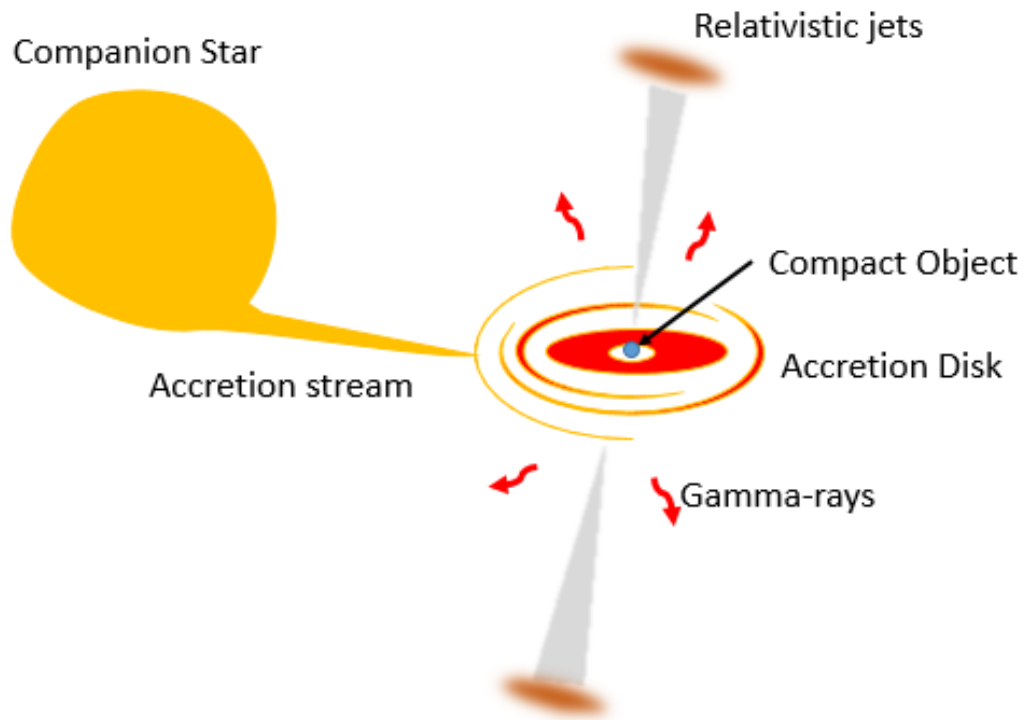


FIGURE 1.4: Microquasar scenario: Massive star accreting material from a compact object(NS/BH). There is an emission of relativistic jets as well.

Many details of gamma-ray binaries are unknown: The nature of the compact object in most of the cases and the origin of the emission: accretion or rotational driven.

The study of temporal behaviour of the gamma-ray emission may provide understanding of the emission mechanisms.

Chapter 2

Imaging Atmospheric Cherenkov Telescopes

This thesis studies the gamma-ray binaries HESS J0632+057 and LMC P3 with H.E.S.S. In this chapter an introduction to Imaging Atmospheric Cherenkov Telescopes (IACTs) in general and H.E.S.S. in particular is given.

2.1 How IACTs operate

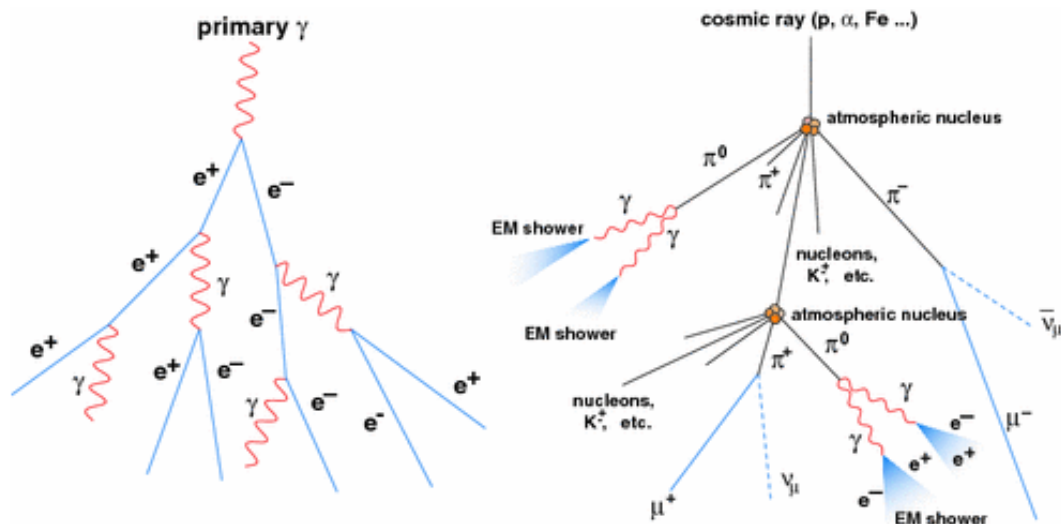


FIGURE 2.1: Left: Primary gamma ray generating Electromagnetic shower. Right: Hadronic particle generating hadronic cascade. Credit: https://link.springer.com/chapter/10.1007/978-88-470-2688-9_4#citeas

Radiation, which is emitted everywhere in the universe, can be detected by both direct and indirect methods. Gamma rays can be detected directly by space-based instruments or indirectly by ground-based instruments. When

VHE gamma rays or Cosmic rays enter the atmosphere, an extensive air shower is formed where the nuclei of the particles in the atmosphere interact with the primary particles. Two types of cascades are formed based on the nature of the primary particle. If the primary particle is a VHE gamma ray, an Electromagnetic shower will be formed, while if the primary particle is a proton/nuclei then a Hadronic shower will form (see Figure 2.1).

Electromagnetic shower

When a VHE gamma ray enters the atmosphere, it undergoes pair production which is the creation of an electron and a positron when the gamma rays interacts with the Coulomb field of the nuclei of the particles in the atmosphere. Electrons and positrons undergo Bremsstrahlung¹ process to emit gamma ray photons. If the radiation has enough energy it will trigger a cascade of particles triggering more photons which themselves can then undergo pair production until the photon energy is below 1 MeV. The development of this cascade is described by a Heitler Model (Matthews, 2005). The development of the cascade stops when the atmosphere absorbs the secondary particles.

Hadronic shower

For the development of this shower, a primary particle (proton/nuclei) interacts with the nuclei found in the atmosphere. The dominant particles in this shower are pions and other mesons. This shower is broader and irregular as compared to the EM shower. A variety of secondary particles initiate the production of secondary particles depending on the amount of the energy available. Pions decay into gamma rays or muons, electrons and neutrinos (see Figure 2.1).

¹Bremsstrahlung: Deceleration of an electron as it is deflected by the nucleus of an atom

2.2 IACTs

Both these two extensive air showers, the electromagnetic shower and the hadronic shower, have particles that are travelling through the dielectric medium at a speed greater than the speed of light. As these particles move, they produce a flash of blue light which is known as Cherenkov light. Pavel Cherenkov first detected the Cherenkov radiation in 1934 and his discovery led to the invention of the Imaging Atmospheric Cherenkov Telescope (IACT). The Cherenkov light flash lasts about 3 to 4 ns.

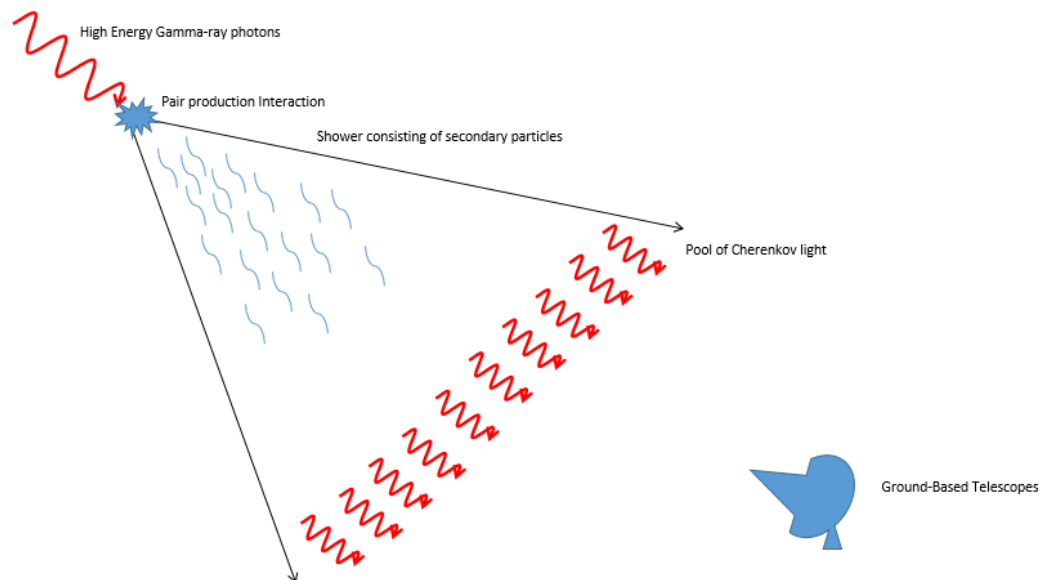


FIGURE 2.2: Depiction of the operation of Imaging Atmospheric Cherenkov Telescopes (IACTs).

IACT is a method aimed at detecting Very High Energy gamma ray photons ranging from 50 GeV-50 TeV. This method is depicted in Figure 2.2. When a gamma ray reaches the atmosphere, an electromagnetic shower forms. The produced charged particles form a cascade thus producing a flash of Cherenkov radiation at an altitude of 10-20 km. The ground-based telescopes then detect the radiation in the optical band and create a visual representation of the shower. IACTs make images of the shower and the images point in the direction of the origin of the gamma ray (Figure 2.3). Multiple images of the same shower allow a stereoscopic reconstruction of the shower and that is the reason we use several telescopes.

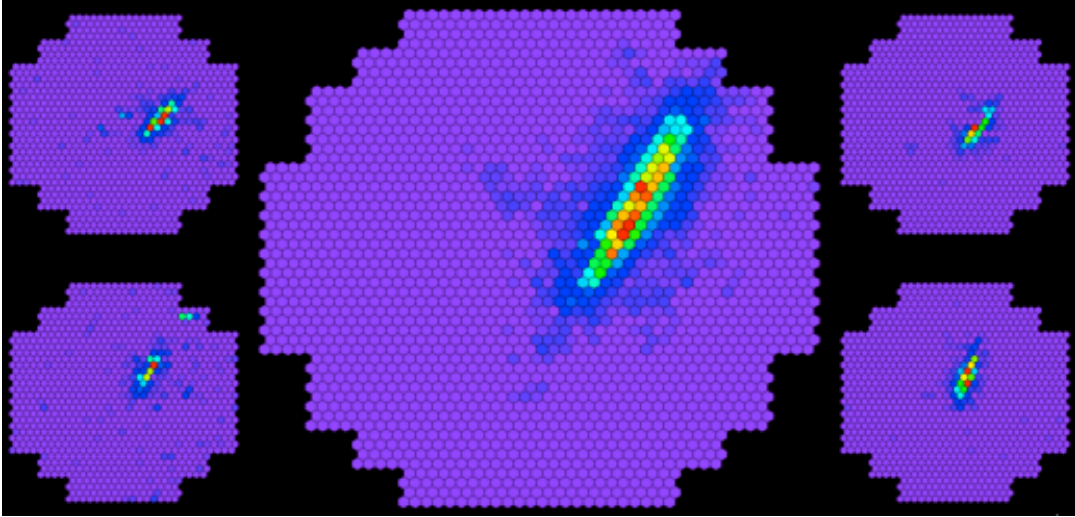


FIGURE 2.3: Camera images of the Extensive Air Shower as viewed on the 5 HESS telescopes. Credit: <https://www.mpi-hd.mpg.de/hfm/HESS/pages/home/som/2012/12/>

2.3 Imaging Atmospheric Cherenkov Telescope instruments

2.3.1 History

In 1968, the first emerging Cherenkov telescope to detect gamma rays was built which is Whipple. It is a 10m diameter telescope located at Mount Hopkins, Arizona in the United States (Kildea, 2007). This telescope in 1989 became the very first to detect VHE gamma rays coming from the Crab Nebula (Weekes et al., 1989). HEGRA with a lifetime from 1997-2002, improved the technology and pioneered the stereoscopic observation (Daum, 1997). In the 2000's, other telescopes following HEGRA were implemented and IACT systems were built and started operating.

The IACT systems built on the concept of HEGRA are:

1. High Energy Stereoscopic System (H.E.S.S).
2. Very Energetic Radiation Imaging Telescope Array System (VERITAS).
3. Major Atmospheric Gamma-ray Imaging Cherenkov (MAGIC).

Current IACTs have effective areas of $\geq 10^5 \text{m}^2$, energy range of $\sim 100 \text{GeV}$ to 30TeV , energy resolution of $\sim 15\% - 20\%$ and an angular resolution of $\approx 0.1^\circ$. They have high sensitivity which enables an observation time of about 30 hours to detect several percent of the flux of the Crab Nebula, which is the

calibration standard candle for all the IACT's (Aliu et al., 2014).

2.3.2 H.E.S.S

H.E.S.S is a system of five Imaging Atmospheric Cherenkov Telescopes which are ground based detectors used for investigating cosmic rays from the energy range of 0.03-100 TeV. It is named in honour of Victor Hess who was the first to discover the behaviour of Cosmic Rays. It is located in the Khomas Highland, Namibia ($S23^{\circ}16'18''$ $E16^{\circ}30'00''$), and includes four, 13m diameter telescopes (in a square formation with 120 m side lengths) and one 28m diameter telescope which is located at the centre of the array of the 4 smaller telescopes. Each of the four smaller telescopes has 107m^2 spherical mirrors. They operate by focusing onto the camera the flashes of Cherenkov light with a Field of View of about 5 degrees in diameter (Bernloehr, 2003).

These detectors are optical telescopes designed to observe the Cherenkov flash since they have a mirror for collecting light and focusing it on a camera. The angular resolution of $\sim 0.1^{\circ}$ which is provided by the stereoscopic technique gives a low energy threshold of $\sim 100\text{GeV}$ for H.E.S.S and allows 1% Crab flux source detection in ~ 25 hours of observations (Benbow and Collaboration, 2005).

The shower model is pre-calculated leading to no cleaning or parametrization of the image. Model analysis is a reconstruction technique for IACTs which compares predictions obtained from a semi-analytical model to raw Cherenkov camera pixel images of an electromagnetic shower (De Naurois and Rolland, 2009).

2.3.3 VERITAS

VERITAS is an IACT that was built in 2007. It is located at Mount Hopkins Arizona USA ($N31^{\circ}40'30''$ $W110^{\circ}57'07''$), and consists of four, 12m telescopes

that are located 100m apart (Holder et al., 2006; Staszak et al., 2015). It went through maintenance in summer 2009 and summer 2012 to improve the sensitivity (Holder, 2015). Its energy resolution at 1 TeV is 17%, the peak effective area is 100 000 m² and the angular resolution at 1 TeV is 0.008° and at 200GeV it is 0.13°.

2.3.4 MAGIC

MAGIC has two IACT telescope dishes of 17m diameter. It is located in Spain on the Canary Island of La Palma. It is equipped with a photomultiplier camera of 3.5° field of View. It has a precision of $\sim 2'$ for localizing the gamma ray sources in the sky (Albert, 2006a).

2.4 Analysis Method

2.4.1 Theta squared plot

Theta variable is is the angular distance between the position of the source and the reconstructed arrival direction of the gamma ray. Figure 2.4 shows how the theta variable is reconstructed. A theta squared plot was generated for detection of the source, it shows the number of events in bins of theta squared. It is called a theta squared plot because it shows the distribution of the squared angular distance of the background events and the γ -ray signal. The background is estimated from similar regions in the camera where no emission is expected (Berge, Funk, and Hinton, 2006). A statistical significance of the source of $> 5\sigma$ is considered a detection.

2.4.2 How ON and OFF sources are obtained

The number of on-source counts, N_{on} , is obtained from counting all gamma-ray candidates coming from a region around the expected source position. The number of off-source counts, N_{off} , is obtained from counting all gamma-ray candidates in control regions in the camera having the same distance from the camera centre as the source. Typically, there are several off-source

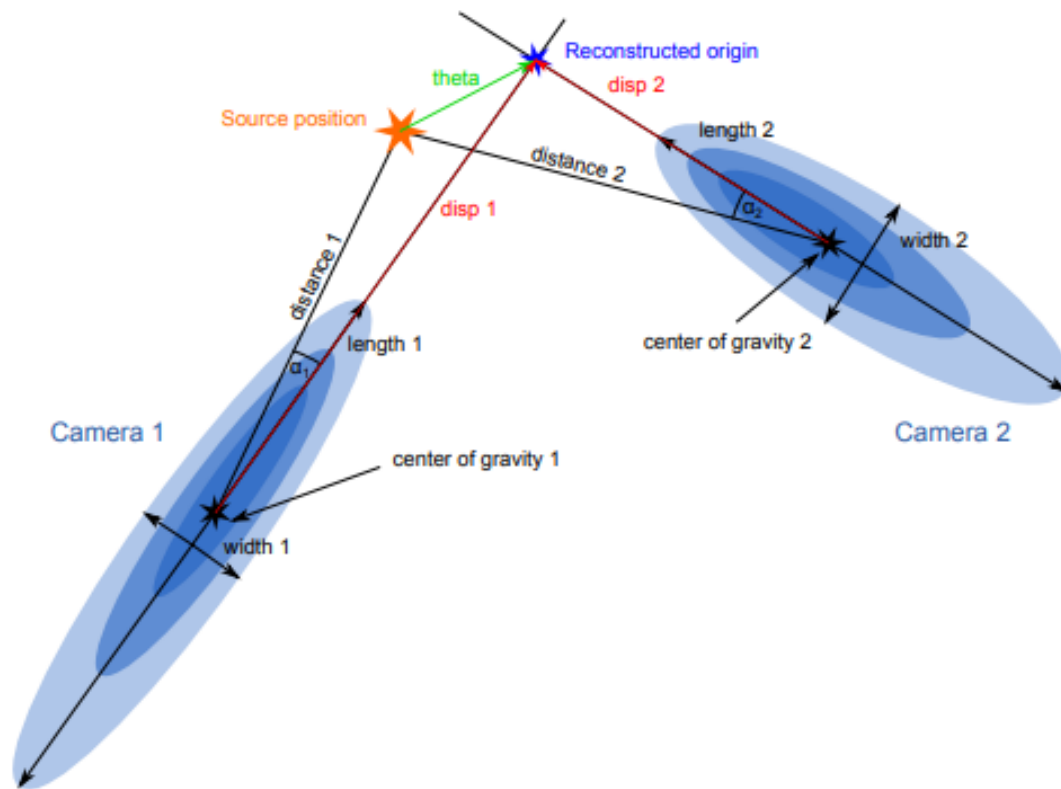


FIGURE 2.4: How the theta parameter is calculated. Credit: (<https://indico.mpp.mpg.de/event/3707/session/14/contribution/51/material/slides/0.pdf>)

regions. The parameter alpha is the ratio between the surface areas of the on-source region and the sum of all off-source regions (Li and Ma, 1983).

2.4.3 Sky Map

The sky map is the second plot used in this analysis. The plot shows the spatial distribution of events. If there is a significant number of events (photons) from the direction of your target, the target can be seen.

2.4.4 Spectrum

The differential energy spectrum shows the distribution of photons with energy. It is described by this equation:

$$\frac{d\phi}{dE} = \left(\frac{dN}{dSdt dE} \right) \quad (2.1)$$

where N is the number of gamma rays, dS is the effective area, dt is the effective observation time, dE is the energy and it typically has the units $\text{cm}^{-2}\text{s}^{-1}\text{TeV}^{-1}$.

The integral flux above a threshold energy E_x can be calculated as:

$$\phi_{E>E_x} = \int_{E_x}^{\infty} \frac{d\phi}{dE} dE \quad (2.2)$$

where its units are normally $\text{cm}^{-2}\text{s}^{-1}$

The simplest spectrum in gamma-ray astronomy is described by a power law:

$$F(E) = \frac{d\phi}{dE} = F_0 \left(\frac{E}{1\text{TeV}} \right)^{-\Gamma} \quad (2.3)$$

This shows the rate of γ rays found per unit area, with units of $\text{cm}^{-2}\text{s}^{-1}\text{TeV}^{-1}$

2.4.5 Light-curve

An integrated light-curve is the evolution with time of an integral flux (ϕ vs t). For this work the energy threshold E_x was set to 350 GeV.

In this work the lightcurve data points were generated on an observational period basis. HESS observation periods start soon after full moon and last until the next full moon, with a duration of about 28 days. The results of all observations from one observational period are combined into one data point.

Given an observation of a binary star, there are enough data points that show a trend of up and down variations showing periodic modulations. However, there is only a few data points (few observations) for each cycle which makes it difficult to tell what the shape of the cycle is. Now to have a better feel of the shape of the cycle, all the cycles can be superimposed on top of each other thus plotting each data point against its distance into the cycle.

In this way, a phase-folded light-curve² arises as a plot of magnitude against function of phase; showing cycles folded on top of each other. The phase is the distance of the data points into the cycle. When plotting the light curve, the standard phase for any time t is computed from period P and epoch t_0 . Phase-folded light curves are shown in Section 4.

²<https://www.aavso.org/sites/default/files/Chapter12.pdf>

Chapter 3

The Gamma-Ray Binaries

HESSJ0632+057 and LMC P3

In this chapter the current knowledge of these two objects is presented.

3.1 HESS J0632+057

Supernova remnants have been recognised as particle accelerators due to the emission of VHE gamma rays and non-thermal X-rays. There have been suggestions that gamma-ray emission should be produced from particle accelerations in interaction of the shell of the supernova remnant (SNRs) with a molecular cloud (Ellison and Bykov, 2011). Because of this, the Monoceros loop and the Rosette Nebula became prime targets of observation. The Monoceros loop is a SNR located at ~ 1.6 kpc from the Earth (Graham et al., 1982). The Rosette Nebula is a young stellar cluster. The interaction between the SNR and the monoceros loop has led to the Monoceros loop being observed for possible VHE gamma rays (Aharonian et al., 2004).

The Monoceros loop (Figure 3.1) was observed from March 2004 to March 2006 with the H.E.S.S. telescopes. In this data set a new source with a statistical significance of 7.1 sigma was found. This source is named HESS J0632+057. It is a point-like gamma-ray source, not related to the Monoceros or Rosette nebula (Aharonian, 2007). This source is coincident with the EGRET source 3EG J0634+0521 (Bongiorno et al., 2011). No significant source variability was detected.

The Swift-XRT Observatory conducted observations on the source in the 0.3-10 keV energy band. The observations extended from 16 January 2009 (MJD = 54857.1) to 27 March 2011 (MJD = 55647.6). The aim of these observations was to test the hypothesis that HESS J0632+057 is indeed a gamma-ray binary star. For this to be true, a periodicity from orbital flux modulations must be confirmed. A period of 321 ± 5 days was detected with a false detection probability $P < 1 \times 10^{-9}$ and Monte Carlo simulations were used to estimate the significance of the proposed period. HESS J0632+057 was then confirmed as the 4th TeV binary (Bongiorno et al., 2011).

VERITAS observed HESS J0632+057 at energies above ≈ 200 GeV from December 2006 - January 2015 for 200 hours (Maier, 2015, Abeysekara, 2015) and there was no detection of significant emission. In 2010-2011, clear gamma ray signals were observed and these signals confirmed the variability of the source in the TeV band (Aliu et al., 2014). This observation resulted in associating the binary star with a few point sources, a weak X-ray source from ROSAT, a massive star and an unidentified lower energy gamma-ray source which is 1RXS J063258.3 + 054857, Be-star MWC 148 and 3EG J0634+0521, respectively (Bordas et al., 2013).

The VERITAS and MAGIC telescopes also confirmed significant variability of the source during their observations, providing evidence on timescales of months for variability of the gamma-ray flux (Bongiorno et al., 2011). For clearer detection optical spectrometric observations were used to determine whether HESS J0632+057 is indeed a binary star (Casares et al., 2012). Jogler et al. (2012) compared HESS J0632+057 with LS I +61 303 and found similarities between their spectral properties for X-ray and flux variability suggesting that it is indeed a member of the class of gamma-ray binaries. Amongst all the known gamma-ray binary stars¹, it is the only one that allows ground-based observations in the Northern and Southern Hemisphere because its location in the sky suits both (Aliu et al., 2014).

¹Abeysekara et al. (2020) confirmed a detection of LS 5039 from the Northern Hemisphere.

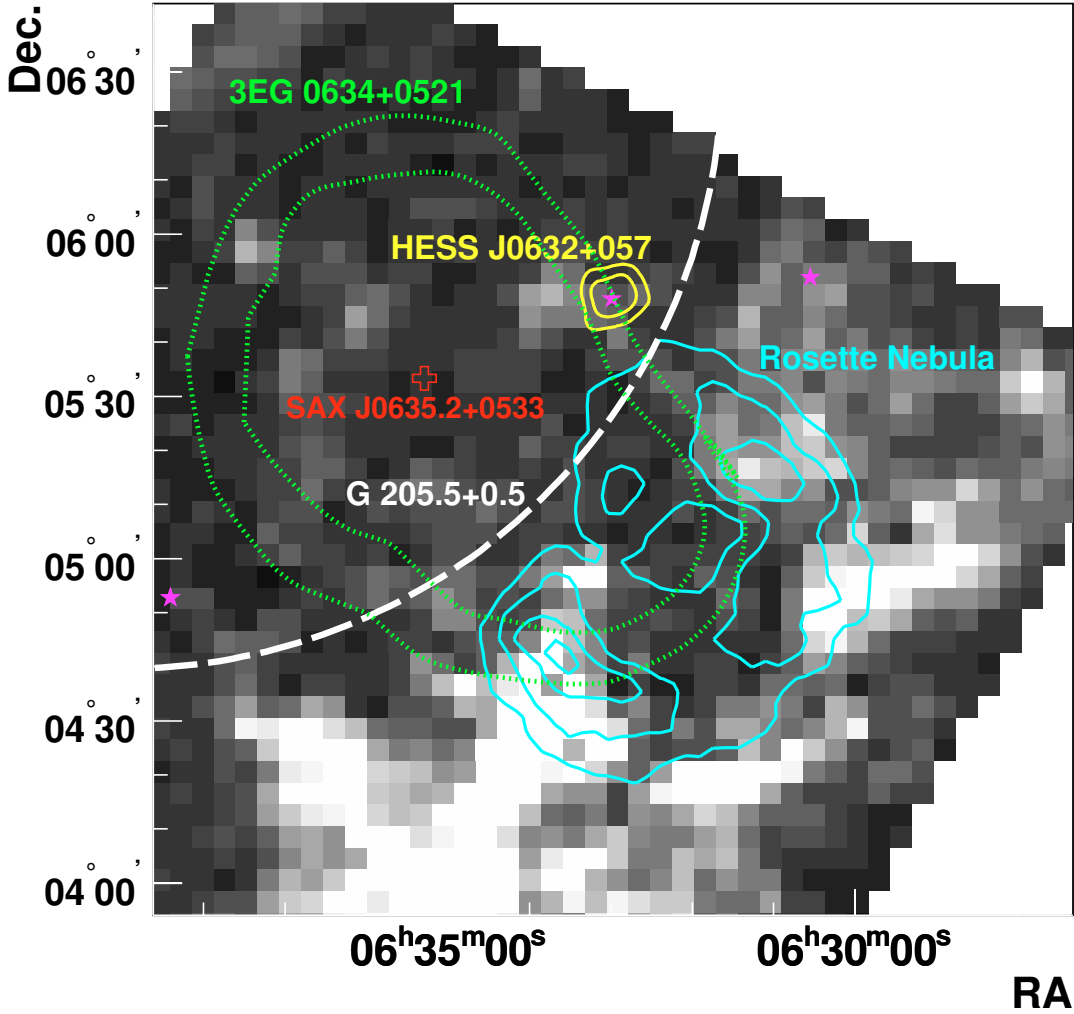


FIGURE 3.1: HESS J0632+057 coincident with MWC 148 located within the Monoceros Loop on the edge of the Rosette Nebula, (Aharonian, 2007)

In Figure 3.2 we can see the geometry of the gamma-ray binary orbit. The figure was constructed using stellar parameters from Aragona, McSwain, and De Becker (2010). The relative motion of MWC 148 and the compact object reveal periastron at an orbital phase 0.967, apastron at an orbital phase 0.467, inferior conjunction at an orbital phase 0.961 and superior conjunction at an orbital phase 0.063 at a period of 321 ± 5 days (Casares et al., 2012) and T_0 of 54857 MJD (Bongiorno et al., 2011). With these values, the high energy emission of HESS J0632+057 is at 0.967 and very high energy emission is at 0.961. In Figure 3.2, there is a visual presentation of the phases with 0.1 intervals of orbital phase. Moritani et al. (2018) kept on monitoring HESS J0632+057 to get a complete coverage of the phase with a motivation of detecting variability of the line profile at the primary outburst. The variability

in the radial velocity of $H\alpha$ was discussed and an improved orbit was obtained with an eccentricity of 0.6 and three outburst occurring with two after apastron and one after periastron. The radial velocity increased from phase 0.2 to 0.6 for a 321-day cycle. The velocity also had a rapid increase from phase 0.3 to 0.6 with a slower decrease from 0.6 to 0.3. These shows that the predicted orbital period by X-ray activity is longer and the periastron is not on the same side as the one proposed by Casares et al. (2012) but rather on the opposite side.

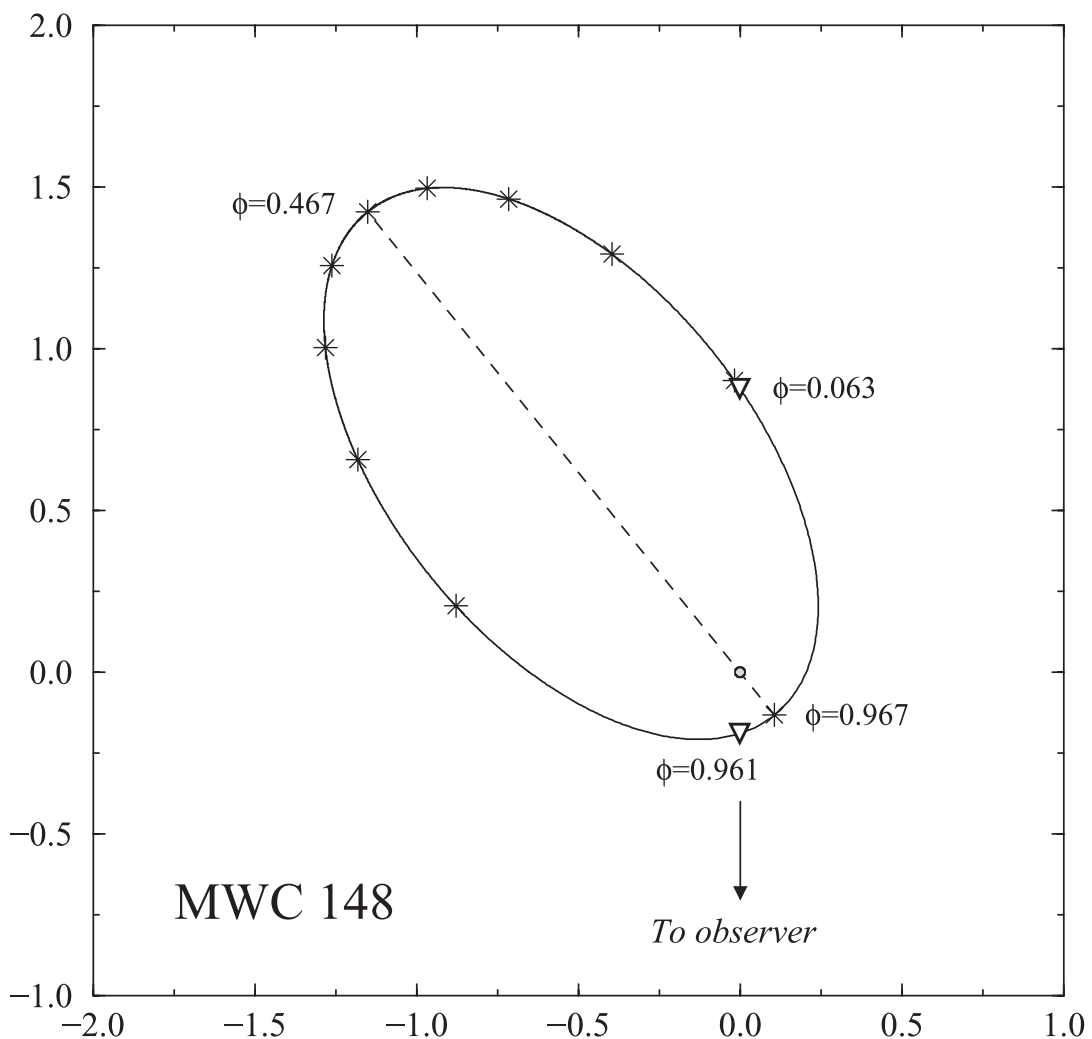


FIGURE 3.2: HESS J0632+057 orbit with periastron phase at 0.967 and apastron phase at 0.467. The dots show 0.1 interval of orbital phase. Credit: Casares et al. (2012)

HESS J0632+057 shows variable gamma-ray emission and periodic X-ray emission. It is associated with a Be star in orbit with a compact object. This makes HESS J0632+057 a gamma-ray binary. The location of the source is on

the edge of the 99% contour of the EGRET unidentified object 3EG J0634+0521, but in the Fermi LAT point source catalogue no object is listed at the position of HESS J0632+057.

Malyshev and Chernyakova (2016) reported on Fermi Large Area Telescope observations of HESS J0632+057. Following a deep search for the gamma-ray emission performed by Li et al. (2017), an unknown gamma-ray source that is believed to be spatially coincident with HESS J0632+057 was discovered. The source is Fermi J0632.6+0548. The measured flux in the energy band ranging from 0.1-300 GeV of Fermi J0632.6+0548 $(0.92 \pm 0.16 \pm 0.08) \times 10^{-11} \text{ erg cm}^{-2} \text{ s}^{-1}$ is consistent with the flux upper limit set by Caliendo et al. (2013) which is $3 \times 10^{-11} \text{ erg cm}^{-2} \text{ s}^{-1}$ of HESS J0632+057.

3.2 LMC P3

The Large Magellanic Cloud is a satellite galaxy of the Milky Way. In Sreekumar et al. (1992) it was reported that the LMC was detected as an extended source by EGRET in the energy range 0.1-100 GeV. Fermi detected an unidentified source with coordinates RA = 83.54 and Decl = -67.54 (Ackermann et al., 2016). The source was named LMC P3. However this source showed no evidence of variability .

Corbet et al. (2016) performed a search for periodic emission for all sources in the Fermi 3FGL catalog. Periodic emission from LMC P3 with a period of 10.301 ± 0.002 days was found. This source was identified with CXOU J053600.0-673507. Here and in the following the orbital phase is defined for a period of 10.301 days and a reference time of 57410.25 ± 0.34 MJD corresponding to the maximum of HE emission. It makes it the first extra-galactic gamma-ray binary and the most luminous known so far.

H.E.S.S detected VHE gamma-ray emission from this source with a significance of 6.4σ . These observations were carried out from 2004 to 2016 with

with a total exposure time of 100 hours. The folded lightcurve shows a maximum of emission at phases between 0.2 and 0.4 and no emission in the other phase bins. This clearly identifies the VHE source as being the gamma-ray binary LMC P3 as it has periodic modulations. The sensitivity of the telescopes did not allow the periodicity to be detected in the night-by-night lightcurve (HESS Collaboration et al., 2018).

Subsequent optical observations with SALT measured the orbit of the system, the eccentricity, periastron and apastron conjunctions. HE emission is observed over the whole orbit. The measure VHE peaks around the phases of inferior conjunction (van Soelen et al., 2019). The maximum in HE occurs close to superior conjunction.

Chapter 4

Analysis and Results

4.1 Data Sets

4.1.1 HESS J0632+057

CT1-4 are the small H.E.S.S telescopes and CT5 is the big H.E.S.S telescope. HESS J0632+057 was observed from 3 December 2013 to 31 January 2017 using the H.E.S.S full array of CT1-4 and CT5. The HESS J0632+057 data set consists of observations where some runs contained all telescopes and some were taken with different array configurations. These runs were either analysed as CT1-4 ignoring CT5, or as CT5 only when the calibration for CT1-4 was missing.

The data set was divided into two, where the first analysis was from a stereo data set which had HESS I and HESS II¹ data from the four small HESS telescopes (CT1-4) ignoring CT5, and the second was from mono data set which only had runs from the big HESS telescope (CT5), ignoring CT1-4, see Table 4.1. In addition to the data sets discussed here there are further archival data sets that were published before and are not included here.

After selection of quality data and removing the runs influenced by bad weather and malfunctioning hardware, the remaining data sets have live hours of 37.9 hours for stereo data set and 31.9 hours for the mono data set. Stereo data set is analyzed with HESSI_Stereo_Std and the mono data set is analyzed with Mono_safe. HESSI_Stereo_Std is a stereoscopic analysis using

¹HESS II is a phase where H.E.S.S enhanced their detection capability by lowering energy threshold to 30 GeV and to improve the sensitivity (Becherini, Punch, and collaboration, 2012).

information of atleast two triggered telescopes which in this case it uses information from CT1-4. Mono_safe is an analysis that uses information from CT5 only since CT5 allows lowering of the energy threshold of H.E.S.S.

4.1.2 LMC P3

LMC P3 was observed from 15 October 2017 to 03 November 2018 with the full array of CT1-4 and CT5. The quality of the data was then assessed and all the ones that were influenced by bad weather and malfunctioning hardware were removed and the remaining data had an exposure time of 57.2 hours.

TABLE 4.1: Detailed description of the configurations used in the study for the two data sets of HESS J0632+057. For mono data set, new runs were used. They are with the new upgraded "HESSIU" cameras. From the stereo data set, old and new runs were used. Old runs corresponds to the original cameras for the HESSI telescopes.

Conf. analysis	Name of data set	runs	Hours
Mono_safe	mono	(HESSII)	31.9
HESSI_Stereo_Std	stereo	(HESSI) + (HESSII)	37.9

4.2 HESS J0632+057

4.2.1 Theta squared plot

In Figure 4.1 and Table 4.2, the stereo data set went through the Model Analysis Standard cut, the exposure time obtained from our data were 37.9 hours with 738 ON events and 9651 OFF events. In Figure 4.1, the normalization factor between the signal and the background exposure is obtained to be 18.47 and the statistical significance is 8.6σ . This shows that we have detected a gamma-ray source, since the statistical significance is 8.6σ .

For the Mono data set the live time obtained from our data was 31.9 hours with 1360 ON events and 9064 OFF events. In Figure 4.2, the normalization factor between the signal and the background exposure is obtained to be 7.03 with statistical significance of 1.8σ . This shows no detection of gamma rays.

The source is too faint in the mono data set.

TABLE 4.2: VHE γ -ray Statistics of HESS J0632+057. MA - Model analysis. Non - number of events in on source region, Noff - number of events in off source region, alpha - background normalisation, depends on the number of off-source regions.

Analysis	Cuts	Data Set	Non	Noff	α	Excess	Significance
Mono_safe	MA(MonoSafe)	mono	1360	9064	7.03	70.1	1.8
HESSI_Stereo_Std	MA(Standard)	stereo	738	9651	18.47	215.4	8.6

4.2.2 Sky Map

For Sky Maps, see Figure 4.3. Stereo data set was used. It shows that there is a clear excess of gamma-rays with a >8 sigma significance at a location which is spatially co-incident with the location of binary system. With the sky map plot we are able to see that HESS J0632+057 is a point source with a clear emission of γ rays.

4.2.3 Energy Spectrum

Figure 4.4 shows the energy spectrum averaged over the stereo data set. It can be fitted with a power law (see equation 2.3). The fit results are summarised in Table 4.3.

TABLE 4.3: Spectral Parameters of HESS J0632+057

SpectrumPowerlaw	
Analysis	Combined
Photon Index (Γ)	2.26 ± 0.10
Differential flux at 1 TeV [$\text{cm}^{-2}\text{s}^{-1}\text{TeV}^{-1}$] $\times 10^{-13}$	(5.35 ± 0.43)
Integral flux [$\text{cm}^{-2}\text{s}^{-1}$] $\times 10^{-13}$	(4.26 ± 0.49)
Equivalent (χ^2/ndf)	107.3/59

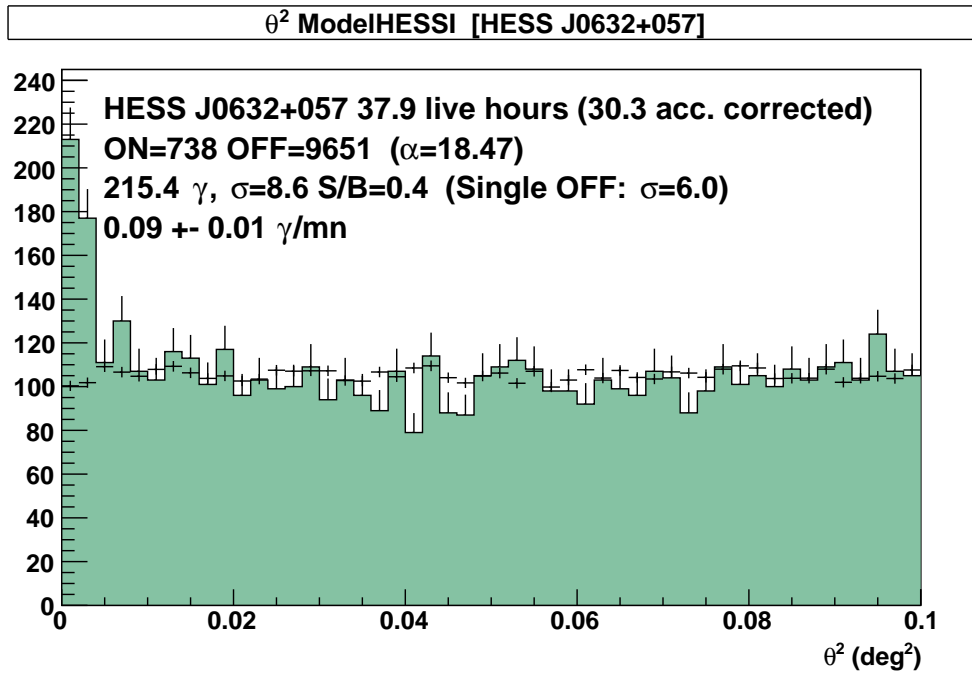


FIGURE 4.1: Distribution of ON(black crosses) and OFF(green shaded region) events from stereo data set HESS J0632+057 and background control regions respectively.

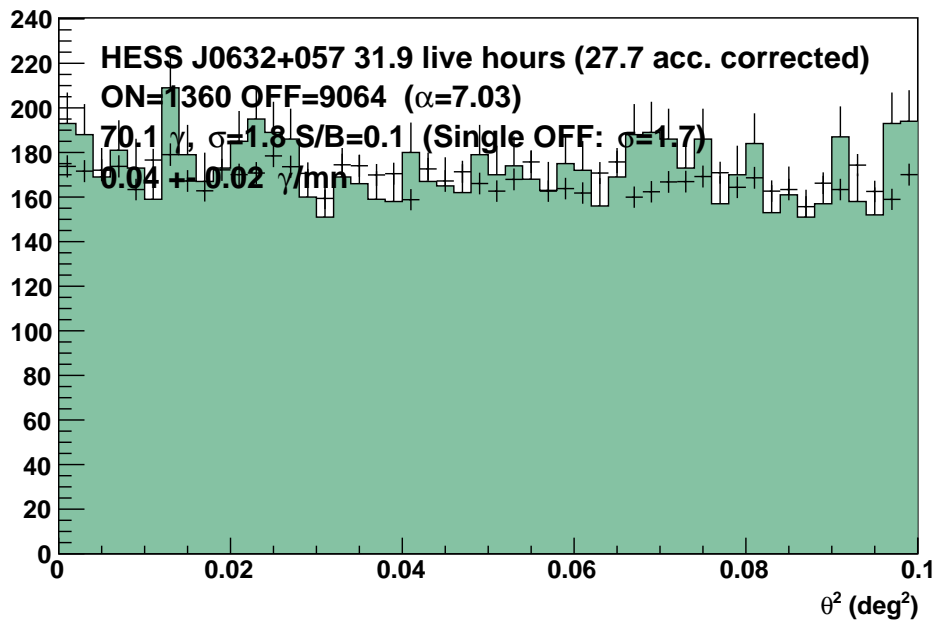


FIGURE 4.2: Distribution of ON and OFF events from Mono data set of HESS J0632+057 and background control regions respectively.

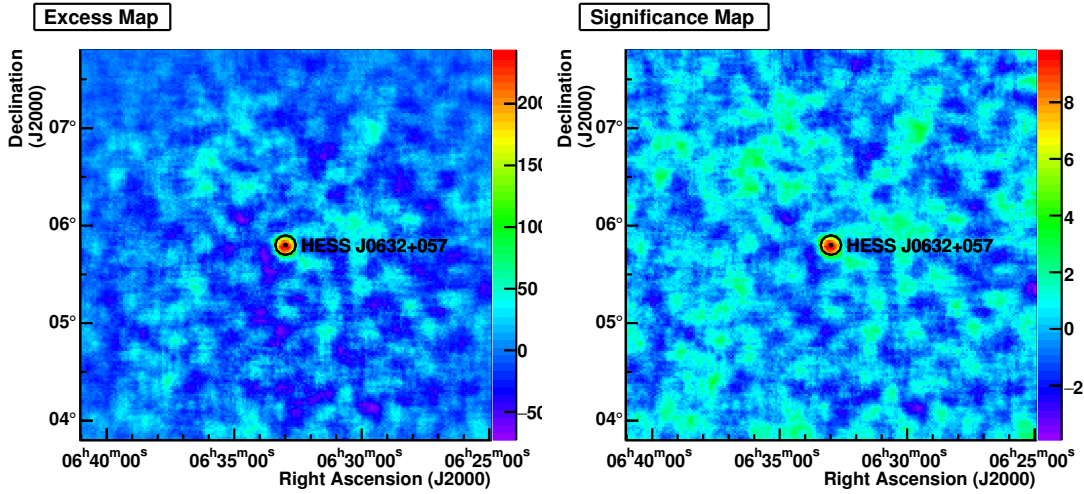


FIGURE 4.3: Sky map showing the location of HESS J0632 +057 with the ON region marked by the black circle on the centre.

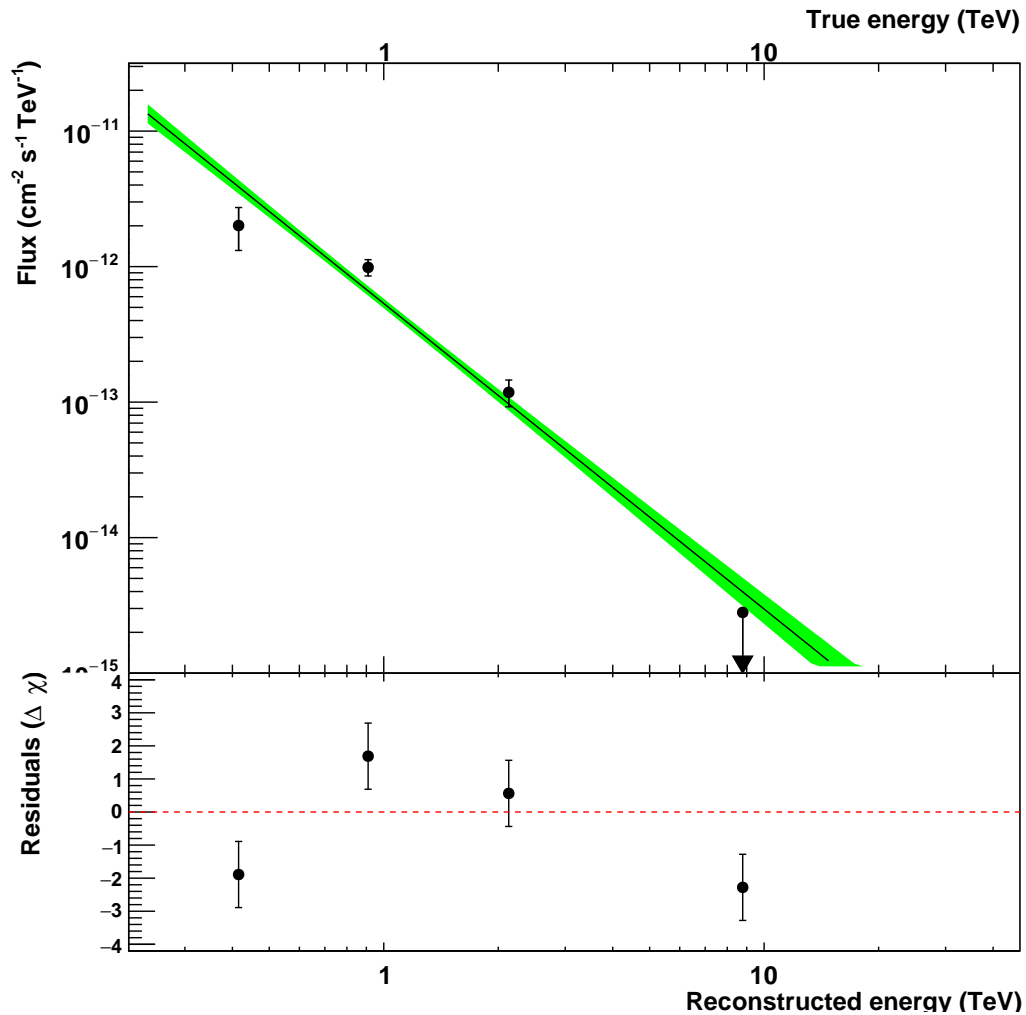


FIGURE 4.4: Observed differential flux of gamma rays in HESS J0632+057. The green line shows the power law fit to the data points used from the stereo data set. A list of the best-fit parameters obtained are listed in Table 4.3

4.2.4 Lightcurve

The integrated lightcurve seen in Figure 4.5 shows that the emission is variable. The phase-folded lightcurve is shown in Figure 4.6. The phase was calculated for a period of 316.2 days and with a phase zero reference time at $T_0 = 54857.0$ MJD. The values were chosen in order to confirm results with VERITAS. From the phase-folded lightcurve, only a single peak is observed between 0.6-0.9.

A constant flux was fitted to the lightcurves, Figure 4.6 and Figure 4.5. The probability of a constant flux was determined from a χ^2 fit and the number of degree of freedom(ndf). As seen in Figure 4.5, the value of $\chi^2 = 35.57$ with (5 degrees of freedom) which gives a probability of $1.158 \times 10^{-6} = 1.58 \times 10^{-4}\%$. This is the probability that a source with constant flux would produce a light-curve with a similar or larger χ^2 . Therefore HESS J0632 is clearly variable.

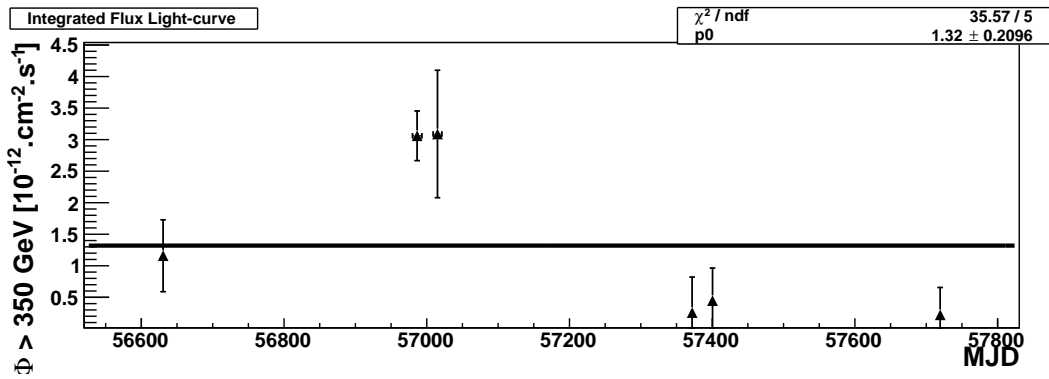


FIGURE 4.5: Integrated lightcurve of HESS J0632+057 computed with energy above 0.35TeV.

4.3 LMC P3

4.3.1 Initial Analysis

LMC P3 was analysed and the first analysis produced a statistical significance of 2.7σ which shows that there is no significant emission, see Figure 4.7. There is 552 ON sources and 19561 OFF sources. The parameters are

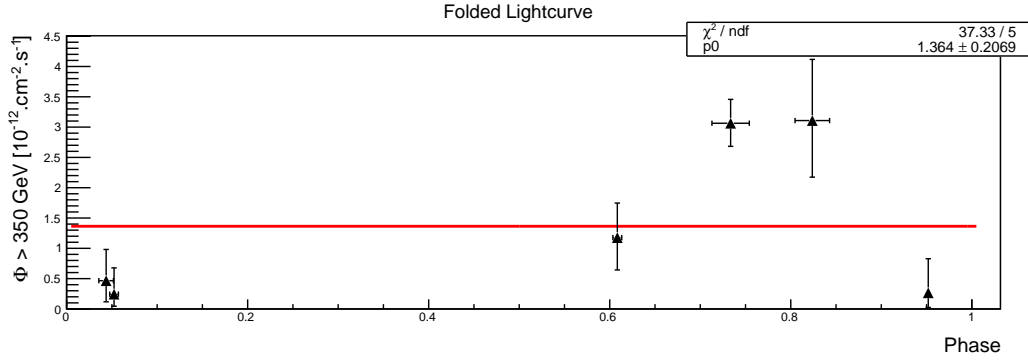


FIGURE 4.6: Phase folded lightcurve of HESS J0632+057 computed with $T_0 = 54857.0$ MJD and $P_0 = 316.2$ days.

presented in Table 4.4. These results were obtained with standard event selection cuts.

With an observation time of almost 60 hours compared to 100 hours in the discovery paper we would expect to see a signal. In order to verify the analysis chain an analysis of the Crab Nebula was performed since this supernova remnant is very bright and is used as a calibration standard for IACT. Figure 4.8 shows the distribution of the mean-scaled shower goodness of the Crab Nebula. The parameters of the plot can be found in Table 4.5. This should follow a Gaussian centered on zero with a width 1. It can be seen that the distribution is displaced by -0.8 instead of being centred at 0 which is the standard configuration of the Model analysis. The mean-scaled shower goodness is used as event selection cut. If the value is too low then too much background will be accepted. Therefore a reduce of the cut by 0.8 was done.

The modified cuts increased the significance from 2.7σ to 3.2σ which is still not enough for a detection, see Figure 4.9.

Figure 4.10 shows the sky map obtained with the reduced event selection cut. Significant emission can be seen, but it is offset from the source position. This clearly indicates a problem with the analysis and that these results are not reliable.

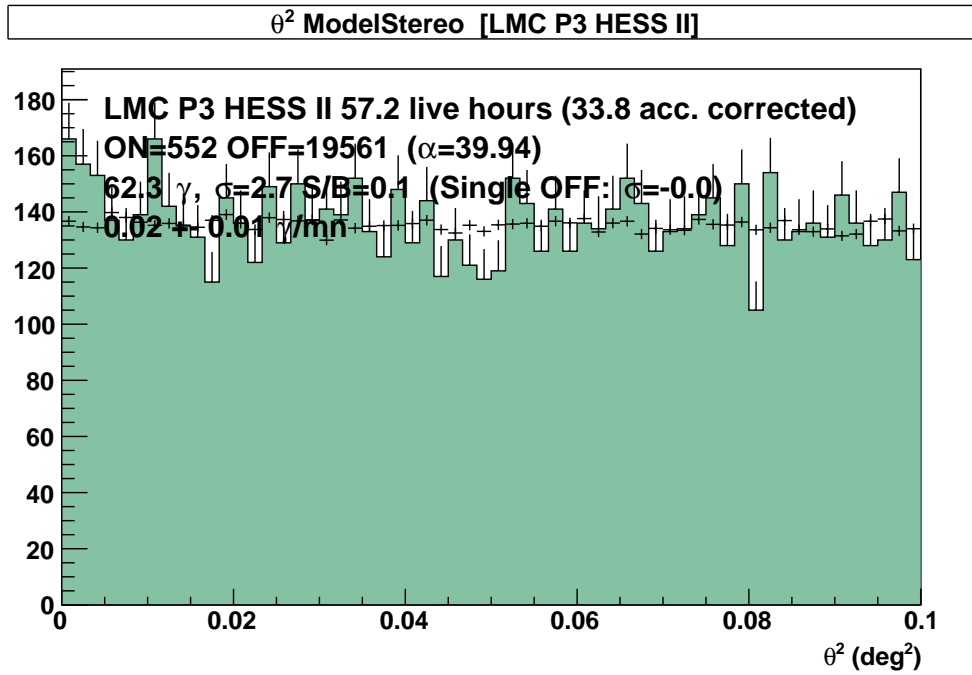


FIGURE 4.7: Theta squared plot of the LMC P3 old instrument response functions with standard shower goodness cut of 0.9. The ON region (black points) and background region (green shaded region) are both distributed in the plot.

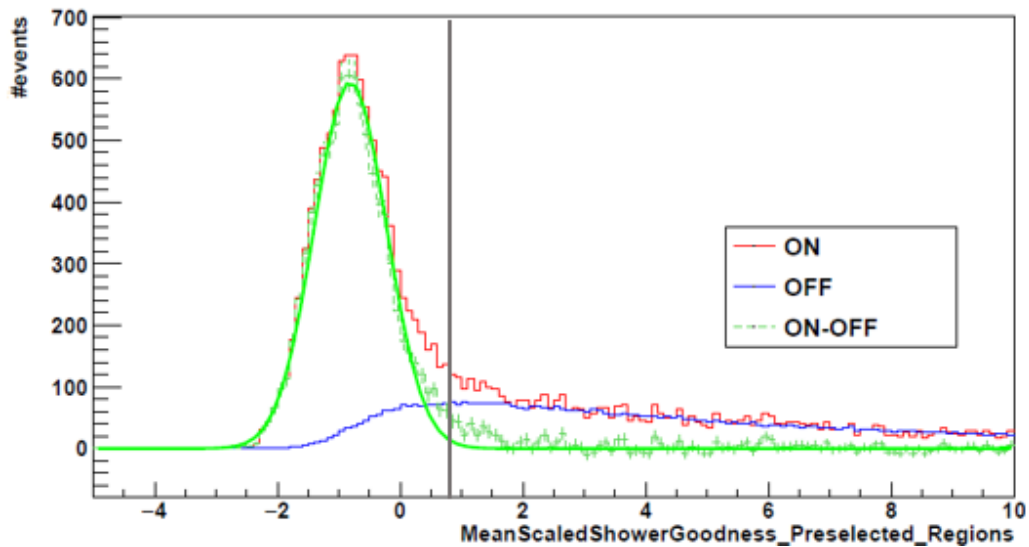


FIGURE 4.8: Distribution of shower goodness of Crab Nebula real data. Red line shows the ON source events, Blue line shows the background and the green line shows the excess events where the OFF source events are subtracted from the ON source events. This shower goodness was computed with H.E.S.S. Paris Analysis old instrument response functions.

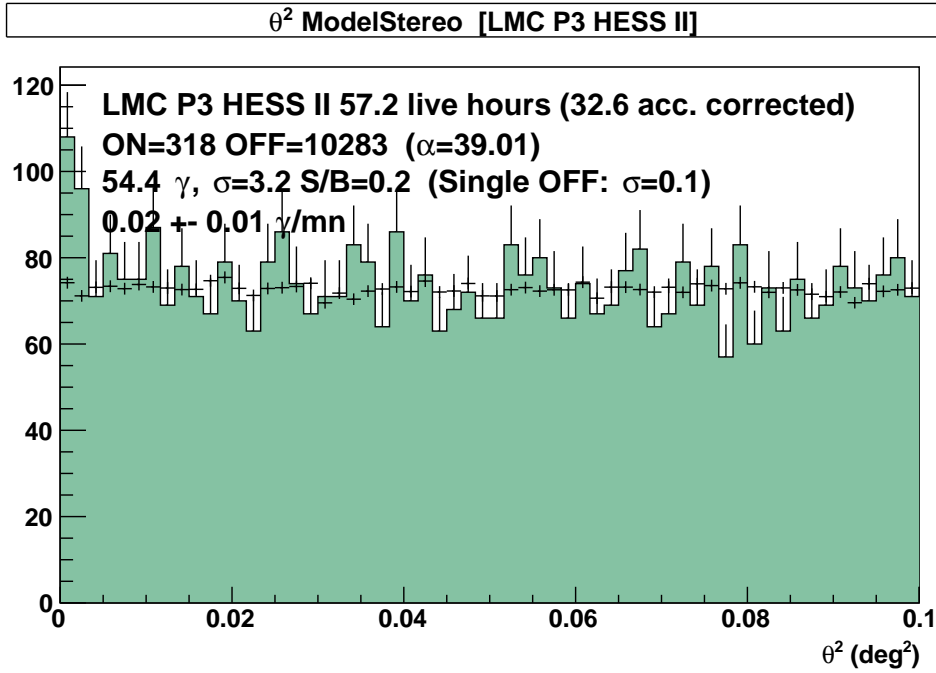


FIGURE 4.9: Distribution of ON(black crosses) and OFF(green shaded region) events from custom analysis of LMC P3 and its background control regions. Reflected background model was used to produce the squared angular distribution.

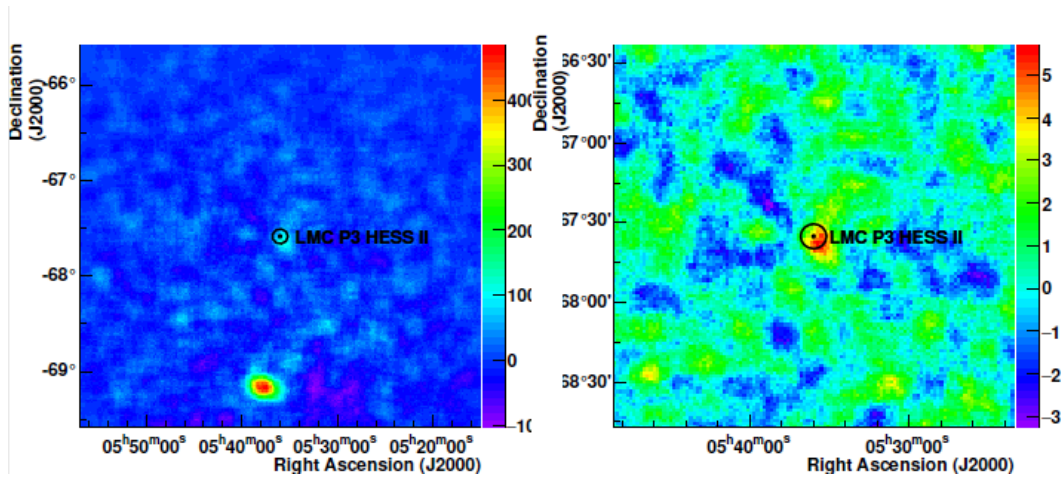


FIGURE 4.10: LMC P3 old instrument response functions sky map showing the location of it with the 'ON' region marked by the black circle on the centre. Left plot is the excess map and the right plot is the significance map

TABLE 4.4: VHE γ -ray Statistics of LMC P3 with standard instrument response functions

Analysis	Non	Noff	α	Excess	σ	live hours
MA(Custom)	552	19561	39.94	62.3	2.7	57.2

TABLE 4.5: Fit values of the mean Shower goodness of gamma rays for Crab Nebula computed with old instrument response functions. The constant corresponds to the amplitude, the mean corresponds to the shift and the sigma corresponds to the width.

Name	Value	Error
Constant	595	8.2
Mean	-0.800	0.008
Sigma	0.590	0.006

4.3.2 Follow-up analysis

Following the discovery of above-mentioned problems H.E.S.S. released a new response function and the analysis was redone. The analysis showed a new problem, namely that the all data recorded by CT5 is not reconstructed. This means in the end that the following analysis only uses CT1-4. Therefore the HESSStd analysis configuration is used.

The live hours obtained from our data were 57.2 hours with 76 ON events and 1300 OFF events. In Figure 4.11, the normalization factor between the signal and the background exposure is obtained to be 26.22 with statistical significance of 3.4.

From the sky map it is also clear that the region of observation has no gamma ray emission (see Figure 4.12).

From the results we can see that the analysis is working, however no significant detection was made. This is not unexpected since the source is too faint to be detected with CT1-4 alone within 57 hours and CT5 would clearly increase the significance. Because of this, it was decided not to continue with the analysis of LMC P3 while there are still technical problems.

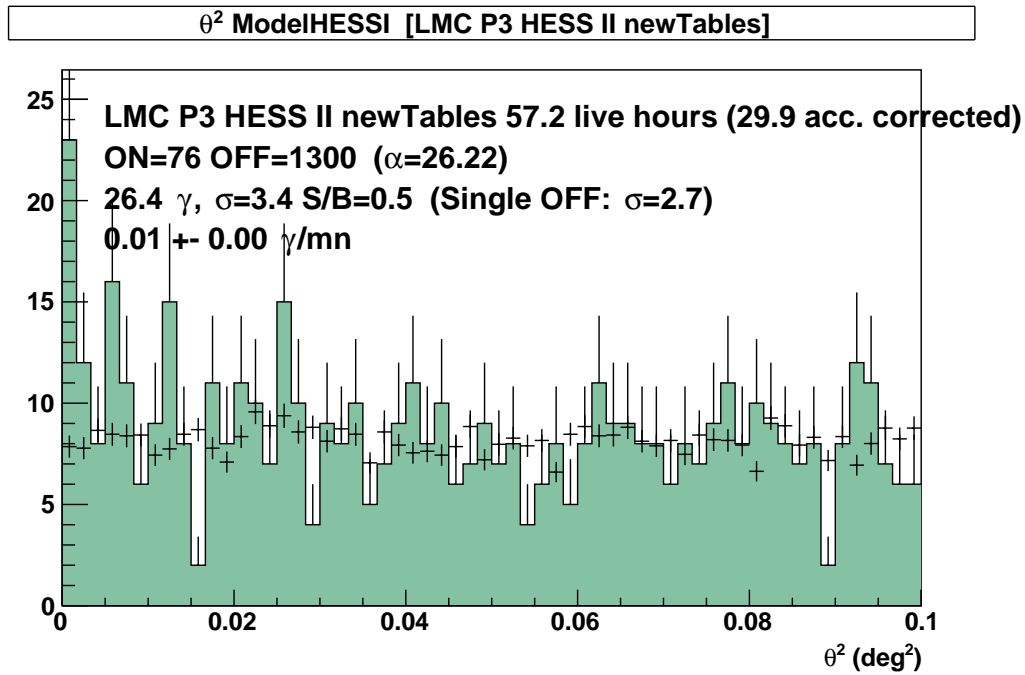


FIGURE 4.11: Distribution of ON(black crosses) and OFF(green shaded region) events from the Stereo_HESSI_standard analysis of LMC P3 and its background control regions with new instrument response functions. Reflected background model was used to produce the squared angular distribution. The theta squared plot is for the modified cuts.

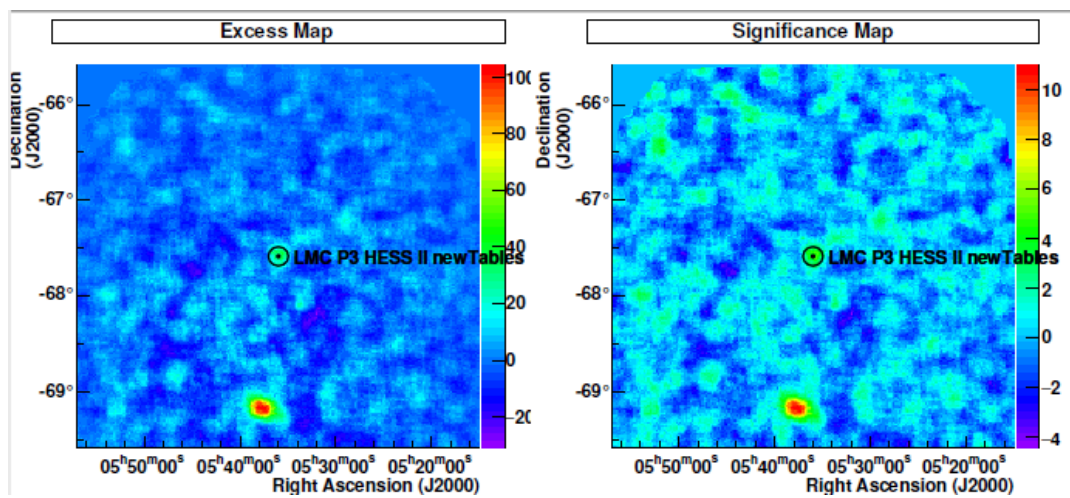


FIGURE 4.12: LMC P3 sky map produced from 4 telescopes showing the location of the source with no gamma-ray detection

Chapter 5

Discussion

5.1 HESS J0632+057

HESS J0632+057 is a variable, point-like source of VHE which is positionally coincident with a Be star. It has properties, such as a hard X-ray spectrum, that suggest the source is a member of the TeV/X-ray binaries class. The main work was to cross-check the H.E.S.S. analysis and to search for a second peak in the light curve. In order to prove the membership of this source in TeV/X-ray binaries, the measurement of the period of the system was done with the combined data set of H.E.S.S. and VERITAS to see if whether it exhibits periodic emission signatures with a period of 316.2 days.

The aim of this research was to do a cross-check analysis of HESS J0632+057 that is to be published by obtaining the spectrum models and light-curves to see if there is a periodic modulation. The analysis was conducted with Model Analysis. With the stereo data set, the statistical significance obtained was 8.6σ . The phase folded lightcurve shows distinct features at 0.3 - 0.4 followed by slight peak at 0.45 then another maximum at 0.75. The dip at 0.45 is believed to be due to shadowing or the suppression of the interaction between the pulsar and stellar winds (Maier, 2012). Aliu et al. (2014) also obtained two distinct periods of the emission at orbital phase 0.3 and a second one between 0.6 and 0.9 and found the source to be variable. In November and December 2017, Archer et al. (2020) performed simultaneous observations in hard X-rays with NuSTAR and TeV gamma-rays with VERITAS. Spectral index from 1.77 ± 0.05 to 1.56 ± 0.05 was observed in X-ray data

and this showed significant variation.

The light-curves were folded with an orbital period of 316.2 days and a reference time of $T_0 = 54857.0$ MJD. HESS J0632+057 was confirmed to have TeV emission by VERITAS and MAGIC in the energy range of 0.35-100 TeV. I cross checked the analysis by setting the energy threshold to 0.35 TeV. These results were shown together with results from VERITAS and MAGIC at the International Cosmic Ray Conference 2019 (Maier et al., 2019). From the analysis of light-curves in the dissertation only the second peak of periodic emission of HESS J0632+057 at VHE is observed. The peak is observed between orbital phases 0.6 and 0.8. The data set presented here does not cover the first maxima at phase 0.3.

The second peak observed was right after apastron but before the inferior conjunction, see Figure 3.2. From a recent publication by the VERITAS collaboration (Maier, 2015), HESS J0632+057 was detected at phases 0.6-0.75 with significance of 9.7σ . The findings in this research confirmed that there is indeed a second maximum at phase 0.6-0.8 with statistical significance of 8.6σ . As the aim was to confirm the results with VERITAS, Figure 5.1 indeed confirms the second maximum.

The probability calculated for the lightcurve, is the probability that a source with constant flux would produce a light-curve with a similar or larger χ^2 . Therefore HESS J0632 is clearly variable.

5.2 LMC P3

The second part of this study was to look at a new H.E.S.S. data set taken on LMC P3 in 2017. Unfortunately, not everything went smoothly and during this work bugs were found in the H.E.S.S pipeline. The old instrument

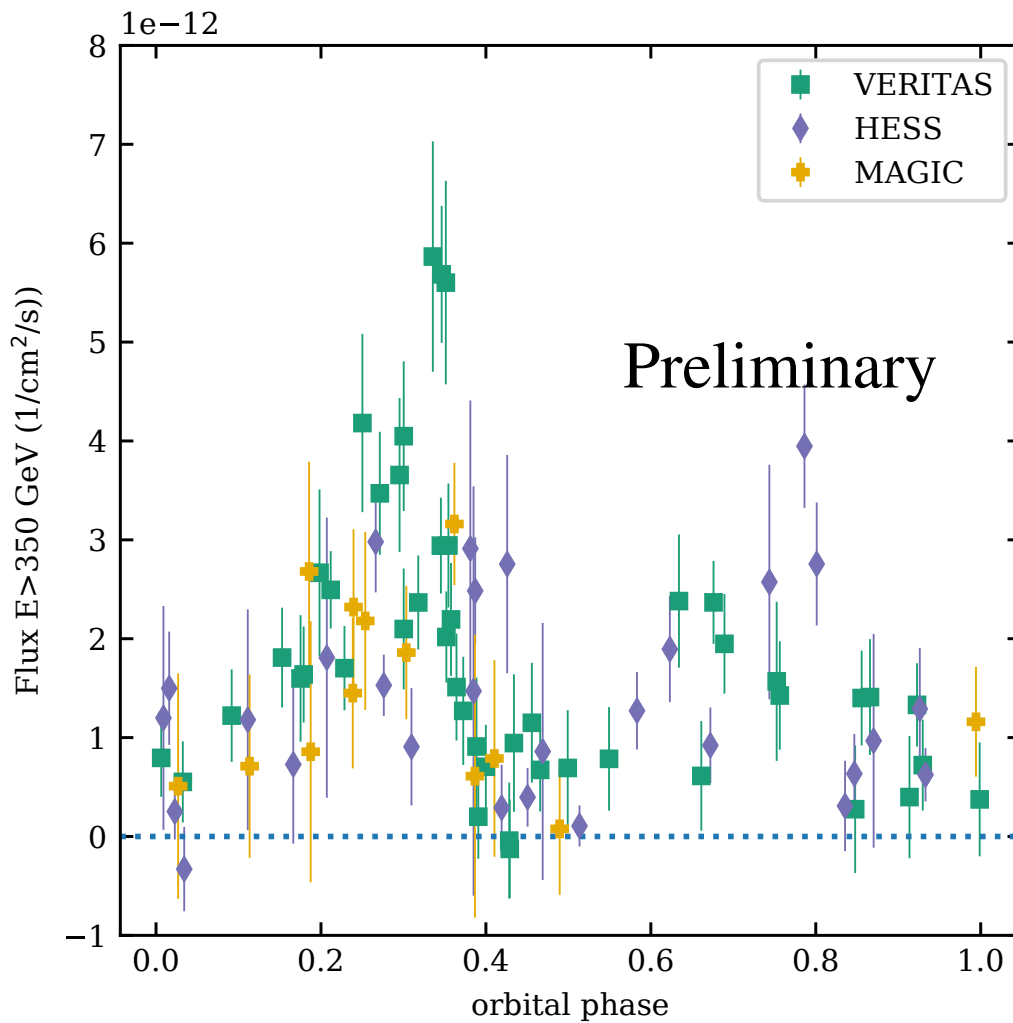


FIGURE 5.1: Published lightcurve from Maier et al. (2019)

response functions are not suited for the new cameras. With the old instrument response functions having an error like this I tried to use the new instrument response functions but these tables seemed to be worse than the old instrument response functions. The problem is that they lost information recorded by CT5, the large 28m telescope. These problems were only solved in June 2019 hence it was not possible to produce reliable results. With this problem, I decided to continue the analysis with the old instrument response functions.

Analysis with the old instrument response functions was backed up by shower goodness plots of the Crab Nebula. The reason for using this supernova remnant was because it is very bright in the sky and the IACTs use it

as a calibration standard candle. From the plot of this supernova remnant, Figure 4.8, we can clearly see the shift in the Model Analysis standard configuration. As stated in Chapter 5, the standard configuration of the distribution of the shower goodness plot is supposed to be a Gaussian centered at 0 with width ranging from [-1,1]. The analysis confirms the error in the scaling of the H.E.S.S Model analysis old instrument response functions, as shown in Figure 4.8 proves it. The parameters of the plot can be found in Table 4.5. From the parameters, the mean value of -0.8 shows that the plot is not centered at 0 but moved 0.8 to the negative direction.

The standard Model++ analysis is performed with the Mean Scaled Shower Goodness set at 0.9. This cut is set as an acceptance value of the gamma rays with limited background. It is a cut that is set for a Gaussian fit centered at 0 with width ranging from [-1,1]. However for the Crab Nebula the Gaussian shifted by -0.8 and the Shower Goodness cut remained at 0.9. This shows that the gamma rays accepted were diluted with the background more than it should be.

In my research I decided to modify the cut by subtracting the 0.8 shift from the 0.9 Mean Scaled Shower Goodness value. I obtained a new SG cut of 0.1. I then restarted the analysis with a new Mean Scaled Shower Goodness value. The statistical significance obtained for LMC P3 computed with matching lookup table and Mean Scaled Shower Goodness of 0.9 was 2.7σ . For the modified shower goodness cut, I obtained a statistical significance of 3.2σ .

Figure 4.10 shows the source in the sky map. The black circle that shows the ON region is not centered on the source region where there is gamma ray emissions. This offset causes less detection of gamma rays. The reason for this offset is not clear, but it seems to be fixed in 2019. The statistical significance is less than 5σ , which is the standard acceptable value of detection.

The new H.E.S.S. Model Analysis instrument response functions have a

problem reading in the data from all 5 telescopes, instead only reading data from the four small telescope. Therefore, it became impossible to analyse the new (after 2016) LMC P3 data with the new instrument response functions because not all the data was going to be analysed. This led to LMC P3 data being computed with the old instrument response functions and modified cut of 0.1.

For the last analysis of LMC P3, I used Model analysis `stereo_HESSI_standard`. This analysis only uses observations from CT1-4. Unfortunately a statistical significance of only 3.4σ was obtained, which falls below the 5σ detection threshold. Therefore, no robust results could be obtained on LMC P3 in this dissertation. However, the discovery of the problems presented in this work allowed the H.E.S.S. Collaboration to address and correct the instrument response functions.

Chapter 6

Conclusion

The thesis has presented H.E.S.S. analysis of two gamma-ray binaries: HESS J0632+057 and LMC P3. The study is based on the analysis of new, unpublished, H.E.S.S data for HESS J0632+057 and LMC P3. The aim was to cross-check the results obtained within the H.E.S.S Collaboration.

The mechanism responsible for powering gamma rays in HESS J0632+057 is not yet known (Bosch-Ramon et al., 2017). This mechanism can only explain the emission at orbital phases at 0.3 and not at 0.6-0.9. However, for new, unpublished, H.E.S.S data for HESS J0632+057 more data needs to be taken so that periodic emission can be observed at phase 0.3. The results obtained show confirmation of the emission peak at phase 0.6-0.9. Therefore more attention must be put on the second maximum of the periodic emission. However there are indeed variability and periodic modulations in HESS J0632+057 with a probability of $1.158 \times 10^{-6} = 1.58 \times 10^{-4}\%$. The results can be further used for the preparation of the conference proceedings and the theoretical implications of these findings are beyond the scope of this work.

Even though modifying the SG cut for analysing the LMC P3 data improved the analysis a little bit, I believe more computations can be done regarding this matter. Firstly the tables can be re-done so as to fix the standard configuration of the Model analysis so that the Gaussian fit will be centered at 0 with shift ranging from [-1,1]. If this issue cannot be solved, there should be enough analysis on modifying the SG cut to fit specific shift of the plot in

a way that the efficiency of the gamma rays is more than the one for background.

Analysing the LMC P3 new data with new calibration tables was not so successful as well. Firstly we know that the new tables do not read data from the large telescope. This case can be solved by re-doing the new tables so that data from the large telescope can be captured and analysed. There also seems to be an issue with LMC P3 new data because I analysed the data with new tables using the `stereo_HESSI_standard`, which is based only on the small four telescopes. With this analysis I hoped for better results because there is data from the 4 telescopes but there was no detection since the significance value was less than 5σ .

Bibliography

- Abdo, A. A. et al. (2009). “Fermi/LAT observations of LS 5039”. In: *The Astrophysical Journal Letters* 706.1, p. L56. URL: <http://stacks.iop.org/1538-4357/706/i=1/a=L56>.
- Abdo, A. A. et al. (2011). “Discovery of High-energy Gamma-ray Emission from the Binary System PSR B1259–63/LS 2883 around Periastron with Fermi”. In: *The Astrophysical Journal Letters* 736.1, p. L11. URL: <http://stacks.iop.org/2041-8205/736/i=1/a=L11>.
- Abeysekara, A. U. et al. (2015). “VERITAS Collaboration Contributions to the 34th International Cosmic Ray Conference”. In: arXiv: [1510.01639](https://arxiv.org/abs/1510.01639) [astro-ph.HE].
- Abeysekara, AU et al. (2018). “Periastron Observations of TeV Gamma-Ray Emission from a Binary System with a 50-year Period”. In: *The Astrophysical Journal Letters* 867.1, p. L19.
- Abeysekara, AU et al. (2020). “VERITAS Detection of LS 5039 and HESS J1825-137”. In: *Astroparticle Physics* 117, p. 102403.
- Abramowski, A. et al. (2015). “Discovery of variable VHE γ -ray emission from the binary system 1FGLJ1018.6–5856”. In: *Astron. Astrophys.* 577, A131. DOI: [10.1051/0004-6361/201525699](https://doi.org/10.1051/0004-6361/201525699). arXiv: [1503.02711](https://arxiv.org/abs/1503.02711) [astro-ph.HE].
- Ackermann, M. et al. (2016). “Deep view of the Large Magellanic Cloud with six years of Fermi-LAT observations”. In: *A&A* 586, A71, A71. DOI: [10.1051/0004-6361/201526920](https://doi.org/10.1051/0004-6361/201526920). arXiv: [1509.06903](https://arxiv.org/abs/1509.06903) [astro-ph.HE].
- Aharonian, F. (2007). “Discovery of a point-like very-high-energy gamma-ray source in Monoceros”. In: *Astron. Astrophys.* 469, pp. L1–L4. DOI: [10.1051/0004-6361:20077299](https://doi.org/10.1051/0004-6361:20077299). arXiv: [0704.0171](https://arxiv.org/abs/0704.0171) [astro-ph].
- Aharonian, FA et al. (2004). “Observation of the Monoceros Loop SNR region with the HEGRA system of IACTs”. In: *Astronomy & Astrophysics* 417.3, pp. 973–979.
- Aharonian, Felix et al. (2005). “Discovery of very high energy gamma rays associated with an X-ray binary”. In: *Science* 309.5735, pp. 746–749.

- Aharonian, Felix et al. (2006). "3.9 day orbital modulation in the TeV γ -ray flux and spectrum from the X-ray binary LS 5039". In: *Astronomy & Astrophysics* 460.3, pp. 743–749.
- Aharonian, F. et al. (2005). "Discovery of the binary pulsar PSR B1259-63 in very-high-energy gamma rays around periastron with HESS". In: *A&A* 442.1, pp. 1–10. DOI: [10.1051/0004-6361:20052983](https://doi.org/10.1051/0004-6361:20052983). URL: <https://doi.org/10.1051/0004-6361:20052983>.
- Albert, J. et al. (2006a). "Variable Very High Energy Gamma-ray Emission from the Microquasar LS I +61 303". In: *Science* 312, pp. 1771–1773. DOI: [10.1126/SCIENCE.1128177](https://doi.org/10.1126/SCIENCE.1128177). arXiv: [astro-ph/0605549](https://arxiv.org/abs/astro-ph/0605549) [astro-ph].
- Albert, Jordi et al. (2006b). "Variable very-high-energy gamma-ray emission from the microquasar LS I+ 61 303". In: *science* 312.5781, pp. 1771–1773.
- Aleksić, J. et al. (2012). "Detection of VHE γ -Rays from HESS J0632+057 during the 2011 February X-Ray Outburst with the MAGIC Telescopes". In: *The Astrophysical Journal Letters* 754.1, p. L10. URL: <http://stacks.iop.org/2041-8205/754/i=1/a=L10>.
- Aliu, E. et al. (2014). "Long-term TeV and X-Ray Observations of the Gamma-Ray Binary HESS J0632+057". In: *The Astrophysical Journal* 780.2, p. 168. URL: <http://stacks.iop.org/0004-637X/780/i=2/a=168>.
- Aragona, C., M. V. McSwain, and M. De Becker (2010). "HD 259440: The Proposed Optical Counterpart of the γ -ray Binary HESS J0632+057". In: *ApJ* 724, pp. 306–312. DOI: [10.1088/0004-637X/724/1/306](https://doi.org/10.1088/0004-637X/724/1/306). arXiv: [1009.2100](https://arxiv.org/abs/1009.2100) [astro-ph.HE].
- Aragona, Christina et al. (2009). "The Orbits of the γ -Ray Binaries LS I+ 61 303 and LS 5039". In: *The Astrophysical Journal* 698.1, p. 514.
- Archer, A. et al. (2020). "Probing the Properties of the Pulsar Wind in the Gamma-Ray Binary HESS J0632057 with NuSTAR and VERITAS Observations". In: *The Astrophysical Journal* 888.2, p. 115. DOI: [10.3847/1538-4357/ab59de](https://doi.org/10.3847/1538-4357/ab59de). URL: <https://doi.org/10.3847/1538-4357/ab59de>.
- Becherini, Yvonne, Michael Punch, HESS collaboration, et al. (2012). "Performance of HESS-II in multi-telescope mode with a multi-variate analysis". In: *AIP Conference Proceedings*. Vol. 1505. 1. AIP, pp. 741–744.
- Benbow, Wystan and HESS Collaboration (2005). "The status and performance of HESS". In: *AIP Conference Proceedings*. Vol. 745. 1. AIP, pp. 611–616.

- Berge, D., S. Funk, and J. Hinton (2006). *Background Modelling in Very-High-Energy-ray Astronomy*.
- Bernloehr, K. et al. (2003). "The optical system of the HESS imaging atmospheric Cherenkov telescopes, Part 1: Layout and components of the system". In: *Astropart. Phys.* 20, pp. 111–128. DOI: [10.1016/S0927-6505\(03\)00171-3](https://doi.org/10.1016/S0927-6505(03)00171-3). arXiv: [astro-ph/0308246](https://arxiv.org/abs/astro-ph/0308246) [astro-ph].
- Bongiorno, S. D. et al. (2011). "A New TeV Binary: The Discovery of an Orbital Period in HESS J0632+057". In: *The Astrophysical Journal Letters* 737.1, p. L11. URL: <http://stacks.iop.org/2041-8205/737/i=1/a=L11>.
- Bordas, P. et al. (2013). "Observations of TeV binary systems with the H.E.S.S. telescope". In: *ArXiv e-prints*. arXiv: [1307.6262](https://arxiv.org/abs/1307.6262) [astro-ph.HE].
- Bosch-Ramon, Valentí et al. (2006). "A microquasar model applied to unidentified gamma-ray sources". In: *Astronomy & Astrophysics* 446.3, pp. 1081–1087.
- Bosch-Ramon, Valentí et al. (2017). "HESS J0632+057: hydrodynamics and non-thermal emission". In: *Mon. Not. Roy. Astron. Soc.* 471.1, pp. L150–L154. DOI: [10.1093/mnrasl/slx124](https://doi.org/10.1093/mnrasl/slx124). arXiv: [1708.00066](https://arxiv.org/abs/1708.00066) [astro-ph.HE].
- C. C. Freire, P. et al. (2012). "Periodic emission from the gamma-ray binary 1FGL J1018.6-5856". In: *Science* 335, pp. 189–193. DOI: [10.1126/science.1213974](https://doi.org/10.1126/science.1213974). URL: <http://hal.in2p3.fr/in2p3-00685309>.
- Caliandro, GA et al. (2013). "The missing GeV γ -ray binary: searching for HESS J0632+ 057 with Fermi-LAT". In: *Monthly Notices of the Royal Astronomical Society* 436.1, pp. 740–749.
- Casares, J. et al. (2005a). "A Possible black hole in the gamma-ray microquasar LS 5039". In: *Mon. Not. Roy. Astron. Soc.* 364, pp. 899–908. DOI: [10.1111/j.1365-2966.2005.09617.x](https://doi.org/10.1111/j.1365-2966.2005.09617.x). arXiv: [astro-ph/0507549](https://arxiv.org/abs/astro-ph/0507549) [astro-ph].
- Casares, J. et al. (2012). "On the binary nature of the gamma-ray sources AGL J2241+4454 (=MWC 656) and HESS J0632+057 (=MWC 148)". In: *Mon. Not. Roy. Astron. Soc.* 421, p. 1103. DOI: [10.1111/j.1365-2966.2011.20368.x](https://doi.org/10.1111/j.1365-2966.2011.20368.x). arXiv: [1201.1726](https://arxiv.org/abs/1201.1726) [astro-ph.SR].
- Casares, Jorge et al. (2005b). "Orbital parameters of the microquasar LS I +61 303". In: *Mon. Not. Roy. Astron. Soc.* 360, pp. 1105–1109. DOI: [10.1111/j.1365-2966.2005.09106.x](https://doi.org/10.1111/j.1365-2966.2005.09106.x). arXiv: [astro-ph/0504332](https://arxiv.org/abs/astro-ph/0504332) [astro-ph].
- Charles, P. A. and Malcolm J. Coe (2003). "Optical, ultraviolet and infrared observations of x-ray binaries". In: arXiv: [astro-ph/0308020](https://arxiv.org/abs/astro-ph/0308020) [astro-ph].

- Corbet, R. H. D. et al. (2012). "Periodic Emission From The Gamma-ray Binary 1FGL J1018.6-5856". In: *American Astronomical Society Meeting Abstracts #219*. Vol. 219. American Astronomical Society Meeting Abstracts, p. 433.01.
- Corbet, R. H. D. et al. (2016). "A Luminous Gamma-ray Binary in the Large Magellanic Cloud". In: *The Astrophysical Journal* 829.2, p. 105. URL: <http://stacks.iop.org/0004-637X/829/i=2/a=105>.
- Corbet, R. H. D. et al. (2019). "Discovery of the Galactic High-mass Gamma-Ray Binary 4FGL J1405.1-6119". In: *The Astrophysical Journal* 884.1, p. 93. DOI: [10.3847/1538-4357/ab3e32](https://doi.org/10.3847/1538-4357/ab3e32). URL: <https://doi.org/10.3847/1538-4357/ab3e32>.
- Corbet, RHD et al. (2011). "1FGL J1018. 6-5856: a new gamma-ray binary". In: *The Astronomer's Telegram* 3221.
- Daum, A. (1997). "First results on the performance of the hegra iact array". In: arXiv: [astro-ph/9704098](https://arxiv.org/abs/astro-ph/9704098) [astro-ph].
- Daum, Andreas et al. (1997). "The HEGRA stereoscopic system of imaging Cherenkov Telescopes". In: *Proc. "Towards a Major Atmospheric Cherenkov Detector V", Kruger Park, SA*.
- De Naurois, Mathieu and Loic Rolland (2009). "A high performance likelihood reconstruction of γ -rays for imaging atmospheric Cherenkov telescopes". In: *As-troparticle Physics* 32.5, pp. 231–252.
- Dubus, G., B. Cerutti, and G. Henri (2010). "The relativistic jet of Cygnus X-3 in gamma rays". In: *Mon. Not. Roy. Astron. Soc.* 404, p. 55. DOI: [10.1111/j.1745-3933.2010.00834.x](https://doi.org/10.1111/j.1745-3933.2010.00834.x). arXiv: [1002.3888](https://arxiv.org/abs/1002.3888) [astro-ph.HE].
- Dubus, Guillaume (2013). "Gamma-ray binaries and related systems". In: *Astron. Astrophys. Rev.* 21, p. 64. DOI: [10.1007/s00159-013-0064-5](https://doi.org/10.1007/s00159-013-0064-5). arXiv: [1307.7083](https://arxiv.org/abs/1307.7083) [astro-ph.HE].
- (2015). "Gamma-ray emission from binaries in context". In: *Comptes Rendus Physique* 16, pp. 661–673. DOI: [10.1016/j.crhy.2015.08.014](https://doi.org/10.1016/j.crhy.2015.08.014). arXiv: [1507.00935](https://arxiv.org/abs/1507.00935) [astro-ph.HE].
- Ellison, Donald C. and Andrei M. Bykov (2011). "GAMMA-RAY EMISSION OF ACCELERATED PARTICLES ESCAPING A SUPERNOVA REMNANT IN A MOLECULAR CLOUD". In: *The Astrophysical Journal* 731.2, p. 87. DOI: [10.1088/0004-637x/731/2/87](https://doi.org/10.1088/0004-637x/731/2/87). URL: <https://doi.org/10.1088/0004-637x/731/2/87>.

- Fazio, G. G. et al. (1968). "An experiment to search for discrete sources of cosmic gamma rays in the 1011 to 1012eV region". In: *Canadian Journal of Physics* 46.10, S451–S455. DOI: [10.1139/p68-268](https://doi.org/10.1139/p68-268). eprint: <https://doi.org/10.1139/p68-268>. URL: <https://doi.org/10.1139/p68-268>.
- Frail, DA and RM Hjellming (1991). "Distance and total column density to the periodic radio star LSI+ 61 deg 303". In: *The Astronomical Journal* 101, pp. 2126–2130.
- Fukugita, Masataka and P. J. E. Peebles (2004). "The Cosmic Energy Inventory". In: *The Astrophysical Journal* 616.2, p. 643. URL: <http://stacks.iop.org/0004-637X/616/i=2/a=643>.
- Graham, DA et al. (1982). "A continuum study of galactic radio sources in the constellation of Monoceros". In: *Astronomy and Astrophysics* 109, pp. 145–154.
- Gregory, PC et al. (1979). "The radio, optical, X-ray, gamma-ray star LSI+ 61 deg 303". In: *The Astronomical Journal* 84, pp. 1030–1036.
- Hadasch, D et al. (2012). "Long-Term Monitoring Of The High-Energy γ -Ray Emission From Ls I+ 61 303 And Ls 5039". In: *The Astrophysical Journal* 749.1, p. 54.
- Hartman, R. C. et al. (1992). "The EGRET high energy gamma ray telescope". In: *NASA Conference Publication*. Ed. by C. R. Shrader, N. Gehrels, and B. Dennis. Vol. 3137. NASA Conference Publication.
- Hermesen, W. (1983). "Gamma-ray sources observed by COS-B". In: *Space Sci. Rev.* 36, pp. 61–92. DOI: [10.1007/BF00171902](https://doi.org/10.1007/BF00171902).
- HESS Collaboration et al. (2018). "Detection of variable VHE γ -ray emission from the extra-galactic γ -ray binary LMC P3". In: *A&A* 610, L17, p. L17. DOI: [10.1051/0004-6361/201732426](https://doi.org/10.1051/0004-6361/201732426). arXiv: [1801.06322](https://arxiv.org/abs/1801.06322) [astro-ph.HE].
- Holder, Jamie (2015). "VERITAS: HAWC's Neighbour to the North". In: *arXiv preprint arXiv:1508.01401*.
- Holder, Jamie et al. (2006). "The first VERITAS telescope". In: *Astroparticle Physics* 25.6, pp. 391–401.
- Jogler, T. et al. (2012). "Recent results from MAGIC observations of the binary systems LS I+61 303 and HESS J0632+057". In: *AIP Conf. Proc.* 1505.1, pp. 370–373. DOI: [10.1063/1.4772274](https://doi.org/10.1063/1.4772274).
- Johnston, Simon et al. (1994). "Radio and optical observations of the PSR B1259–63/SS 2883 Be star binary system". In: *Monthly Notices of the Royal Astronomical Society* 268.2, pp. 430–436.

- Kalogera, V. and R. F. Webbink (1998). “Formation of Low-Mass X-Ray Binaries. II. Common Envelope Evolution of Primordial Binaries with Extreme Mass Ratios”. In: *ApJ* 493, pp. 351–367. DOI: [10.1086/305085](https://doi.org/10.1086/305085). eprint: [astro-ph/9708223](https://arxiv.org/abs/astro-ph/9708223).
- Kildea, J. et al. (2007). “The Whipple Observatory 10-m gamma-ray telescope, 1997–2006”. In: *Astropart. Phys.* 28, pp. 182–195. DOI: [10.1016/j.astropartphys.2007.05.004](https://doi.org/10.1016/j.astropartphys.2007.05.004).
- Li, Jian et al. (2017). “GeV detection of HESS J0632+ 057”. In: *The Astrophysical Journal* 846.2, p. 169.
- Li, T-P and Y-Q Ma (1983). “Analysis methods for results in gamma-ray astronomy”. In: *The Astrophysical Journal* 272, pp. 317–324.
- Maier, G et al. (2019). “Long-term gamma-ray observations of the binary HESS J0632+ 057 with HESS, MAGIC and VERITAS”. In: *arXiv preprint arXiv:1908.03589*.
- Maier, G. et al. (2019). “Long-term gamma-ray observations of the binary HESS J0632+057 with H.E.S.S., MAGIC and VERITAS”. In: *36th International Cosmic Ray Conference (ICRC2019)*. Vol. 36. International Cosmic Ray Conference, p. 732. arXiv: [1908.03589](https://arxiv.org/abs/1908.03589) [[astro-ph.HE](https://arxiv.org/abs/astro-ph.HE)].
- Maier, Gernot et al. (2012). “Observation of binary systems at very-high energies with VERITAS”. In: *AIP Conference Proceedings*. Vol. 1505. 1. AIP, pp. 362–365.
- (2015). “Long-term TeV Observations of the Gamma-ray Binary HESS J0632+ 057 with VERITAS”. In: *arXiv preprint arXiv:1508.05489*.
- Malyshev, D and M Chernyakova (2016). “Constraints on the spectrum of HESS J0632+ 057 from Fermi-LAT data”. In: *Monthly Notices of the Royal Astronomical Society* 463.3, pp. 3074–3077.
- Martí-Devesa, Guillem and Olaf Reimer (2020). “X-ray and gamma-ray orbital variability from the gamma-ray binary HESS J1832-093”. In: *arXiv preprint arXiv:2001.02701*.
- Massi, M. et al. (2004). “Hints for a fast precessing relativistic radio jet in LS I +61 degree 303”. In: *Astron. Astrophys.* 414, pp. L1–L4. DOI: [10.1051/0004-6361:20031760](https://doi.org/10.1051/0004-6361:20031760). arXiv: [astro-ph/0312091](https://arxiv.org/abs/astro-ph/0312091) [[astro-ph](https://arxiv.org/abs/astro-ph)].
- Matthews, J. (2005). “A Heitler model of extensive air showers”. In: *Astropart. Phys.* 22, pp. 387–397. DOI: [10.1016/j.astropartphys.2004.09.003](https://doi.org/10.1016/j.astropartphys.2004.09.003).
- McSwain, M Virginia et al. (2010). “H α Emission Variability in the γ -ray Binary LS I+ 61 303”. In: *The Astrophysical Journal* 724.1, p. 379.

- Mirabel, I. F. (2006). "Very Energetic Gamma-Rays from Microquasars and Binary Pulsars". In: *Science* 312, pp. 1759–1760. DOI: [10.1126/science.1129815](https://doi.org/10.1126/science.1129815). arXiv: [astro-ph/0606393](https://arxiv.org/abs/astro-ph/0606393) [astro-ph].
- Moritani, Yuki et al. (2018). "Orbital solution leading to an acceptable interpretation for the enigmatic gamma-ray binary HESS J0632+057". In: *PASJ* 70.4, 61, p. 61. DOI: [10.1093/pasj/psy053](https://doi.org/10.1093/pasj/psy053). arXiv: [1804.03831](https://arxiv.org/abs/1804.03831) [astro-ph.HE].
- Napoli, Vanessa J et al. (2011). "The Distance of the γ -ray Binary 1FGL J1018. 6–5856". In: *Publications of the Astronomical Society of the Pacific* 123.909, p. 1262.
- Negueruela, Ignacio et al. (2011). "Astrophysical Parameters of LS 2883 and Implications for the PSR B1259-63 Gamma-ray Binary". In: *The Astrophysical Journal Letters* 732.1, p. L11.
- Patterson, J. (1984). "The evolution of cataclysmic and low-mass X-ray binaries". In: *ApJS* 54, pp. 443–493. DOI: [10.1086/190940](https://doi.org/10.1086/190940).
- Postnov, K. A. and L. R. Yungelson (2014). "The Evolution of Compact Binary Star Systems". In: *Living Reviews in Relativity* 17, 3, p. 3. DOI: [10.12942/lrr-2014-3](https://doi.org/10.12942/lrr-2014-3). arXiv: [1403.4754](https://arxiv.org/abs/1403.4754) [astro-ph.HE].
- Shannon, RM, S Johnston, and RN Manchester (2014). "The kinematics and orbital dynamics of the PSR B1259- 63/LS 2883 system from 23 yr of pulsar timing". In: *Monthly Notices of the Royal Astronomical Society* 437.4, pp. 3255–3264.
- Soelen, B van et al. (2019). "The orbital parameters of the gamma-ray binary LMC P3". In: *Monthly Notices of the Royal Astronomical Society* 484.3, pp. 4347–4351.
- Sreekumar, P et al. (1992). "Observations of the Large Magellanic Cloud in high-energy gamma rays". In: *The Astrophysical Journal* 400, pp. L67–L70.
- Staszak, David et al. (2015). "Science highlights from VERITAS". In: *arXiv preprint arXiv:1510.01269*.
- Swanenburg, B. N. et al. (1981). "Second COS B catalog of high-energy gamma-ray sources". In: *ApJ* 243, pp. L69–L73. DOI: [10.1086/183445](https://doi.org/10.1086/183445).
- Tavani, M et al. (1998). "The variable gamma-ray source 2CG 135+ 01". In: *The Astrophysical Journal Letters* 497.2, p. L89.
- Weekes, T. C. et al. (1989). "Observation of TeV gamma rays from the Crab nebula using the atmospheric Cerenkov imaging technique". In: *ApJ* 342, pp. 379–395. DOI: [10.1086/167599](https://doi.org/10.1086/167599).
- Zamanov, RK et al. (1999). "Evidence of H alpha periodicities in LS I+ 61303". In: *arXiv preprint astro-ph/9909233*.